Designed synthesis of mesoporous solids *via* nonionic-surfactant-templating approach

Ying Wan,[ab] Yifeng Shi[a] and Dongyuan Zhao*[a]

Received (in Cambridge, UK) 24th July 2006, Accepted 26th September 2006
First published as an Advance Article on the web 23rd October 2006
DOI: 10.1039/b610570j

The continual needs for improved performances in applications derived by diversified compositions and mesostructures have pushed forward the development of mesoporous solids. The nonionic-surfactant-templating approach has been a critical route in this advancement. A large number of nonionic surfactants widely used in industries and featured with low cost, low toxicity, bio-degradation and ordered microdomains can be utilized as effective templates to the design and synthesis of abundant mesoporous solids. This feature article provides recent reports on the use of nonionic surfactant self-assembly as examples to fabricate high-quality ordered mesoporous solids which illustrates advances in synthesis and understanding of formation mechanisms. It includes the selection of surfactants, a summary of the effects of synthetic parameters, the current understanding of the synthetic pathways and related mechanisms with some emphasis on evaporation induced self-assembly (EISA), as well as the design and synthesis on the microscale (atomic and molecular compositions) and mesoscale (mesostructures). Preliminary applications of mesoporous solids particularly in optical devices, electrodes and biomaterials are also presented.

1 Introduction

In materials science, building blocks play key roles which have controllable properties, as well as ordered, complex and integrated structures.[1,2] For synthetic chemistry, supramolecular assembly represents a powerful methodology in the creation of large, discrete, ordered structures. A large number of materials have been developed, particularly periodic mesoporous solids. They combine liquid-crystal packing with rigid frameworks.[3–5] Exceptional properties of highly ordered mesostructures, *i.e.* their large surface areas and uniform pore sizes endow them with powerful properties with countless potential applications in adsorption, separation, catalysis, photonics, quantum dots, *etc*.[6–8]

The middle 1990s witnessed efforts to increase the number of mesostructures from a nonionic-surfactant-templating approach.[5,9–12] Nonionic surfactants differ from both cationic and anionic surfactants in which the molecules are actually uncharged. The hydrophilic groups are made up of water-soluble moieties, (*e.g.* water-soluble polymer chains) rather than charged head groups. Traditionally, most of nonionic surfactants consist of poly(ethylene oxide) (PEO) chains as hydrophilic groups. They are widely used in industry by reason of attractive characteristics such as low cost, low toxicity and bio-degradation. In addition, nonionic surfactants have a range of ordered microdomain morphologies, and have

[a]*Department of Chemistry, Shanghai Key Laboratory of Molecular Catalysis and Innovative Materials, Key Laboratory of Molecular Engineering of Polymers, Advanced Materials Laboratory, Fudan University, Shanghai 200433, P. R. China. E-mail: dyzhao@fudan.edu.cn; Fax: 86-21-6564-1740; Tel: 86-21-6564-2036*
[b]*Department of Chemistry, Shanghai Normal University, Shanghai 200234, P. R. China*

Ying Wan

Ying Wan completed each of her academic degrees in industrial catalysis from the East China University of Science and Technology, receiving her PhD in 2002 with Professor Jianxin Ma. Then, she joined Shanghai Normal University as an Associate Professor. She is currently a postdoctoral member in Fudan University working with Professor Dongyuan Zhao on mesoporous carbon molecular sieves in catalysis and electrodes.

Yifeng Shi

Yifeng Shi received his BS in Polymer Science from Fudan University in 2000 and received his MS in Materials Physics and Chemistry from Shanghai Institute of Ceramics, CAS in 2003. He is currently a PhD student in the porous materials group of Professor Dongyuan Zhao in Fudan University. His research is mainly focused on the synthesis of mesoporous non-oxide ceramic and semiconductor materials.

become more and more popular and powerful in the synthesis of mesoporous solids. Pinnavaia and co-workers first reported mesoporous silicates templated by organic amines, nonionic oligomeric surfactants and triblock copolymers under neutral conditions and proposed a hydrogen-bonding interaction mechanism, namely N^0I^0 or S^0I^0, where N^0 are neutral amines, S^0 are nonionic surfactants and I^0 are hydrated silicate oligomers derived from tetraethoxy silicate (TEOS).[9,10] The products are disordered worm-like mesoporous materials. The pore size distributions are however, uniform and their hydrothermal and thermal stability are high. Attard *et al.* successfully prepared ordered mesoporous silica structures by using $C_{12}EO_8$ and $C_{16}EO_8$ as structure-directing agents (SDAs) which exhibit pore sizes up to 3.0 nm.[11] Lately, Wiesner and co-workers conducted illuminating work on the preparation of large pore mesoporous ceramics employing poly(isoprene)-*block*-poly(ethylene oxide) (PI-*b*-PEO) block copolymers as SDAs in an acidic and non-aqueous medium.[12] This suggested that the use of high-molecular-weight block copolymer mesophases instead of conventional low-molecular-weight surfactants provides a simple, easily controlled pathway for the preparation of large-pore silicate mesostructures. Highly ordered mesoporous SBA-15 was then synthesized under strongly acidic conditions by using poly(ethylene oxide)-*block*-poly(propylene oxide)-*block*-poly(ethylene oxide) (PEO-PPO-PEO) triblock copolymer P123 ($EO_{20}PO_{70}EO_{20}$) as the SDA.[5] The mechanism is most likely *via* an $S^0H^+X^-I^+$ double-layer hydrogen bonding interaction. Here I^+ are inorganic silicate precursor cations, and X^- are counter-anions.

It is well known that self-assembly occurs when molecules interact with one another through a balance of attractive and repulsive interactions. These interactions are generally weak (that is, comparable to thermal energies) and noncovalent, *e.g.* van der Waals and Coulomb interactions, and hydrogen bonds.[13] Therefore, the nonionic-surfactant-templating route is meaningful. It creates ordered mesoporous silicates based on hydrogen-bonding interaction that is a significant complement to Coulombic interaction between cationic or anionic surfactants and inorganic species.[14] To effectively utilize the abundant knowledge on supramolecular self-assembly and sol–gel chemistry, it is favorable to fully understand formation mechanisms of mesoporous solids.

Remarkable progress in the synthetic chemistry of the nonionic-surfactant-templating approach to mesoporous solids has been developed by many research groups.[5,7,12,15–22] The studies are focused at least on the following three aspects: (1) rationally synthesizing mesoporous materials with desired components and structures, (2) investigating morphologies, pore structures and surface chemistry, and (3) implementing the physical and chemical properties towards applications.

Among the mesoporous solids, ordered mesoporous silicates are mostly widely studied.[23–28] Although the syntheses of ordered mesoporous silicates are seemingly very simple, the products differ from each other if the syntheses are not adequately controlled. This factor is difficult to analyze and limits practical applications of mesoporous silicates. The implied issue is that new family members of mesoporous materials will be created upon the complicated combination of simple synthetic factors. Some factors, though usually neglected, may act as critical factors for the synthesis. Therefore, grasping proper synthesis skills is necessary before gaining most benefit from the research. Fully understanding the role of structure directing agents in the synthesis will obviously benefit for the fabrication of high-quality mesoporous solids and further applications of advanced nanomaterials. Another challenging question for material scientists is whether the elaborate studies on syntheses of mesoporous silicates can be extended to ordered nonsiliceous mesoporous materials.[29,30] For mesoporous nonsiliceous materials, most oxides are disordered or hybrid mesostructures that are more distinct for multi-component mesoporous solids.[18] The reasons may arise from the complexity of reactive properties and chemical stability intrinsic in the desired constituents, as well as the difficult control of hydrolysis, polymerization, cross-linkage and inorganic–organic self-assembly.[22,30,31] Consequently, generalized assembly approaches are important for producing ordered nonsiliceous mesoporous materials, especially in examples with multi-component and 3D channels.

These two aspects of mesostructured solids with different components are inextricably linked, which can be mutually influenced and improved. In fact, the progress in the syntheses of nonsiliceous mesostructures is based on the studies of mesoporous silicates. By carefully manipulating the processing variables such as temperature, pH, ionic strength, reaction time and solution composition, ordered mesoporous solids with diverse structures and adjustable physical properties have been obtained from different nonionic surfactants. In this paper, recent reports are provided on the use of nonionic surfactant self-assembly as examples to demonstrate facile synthesis skills and to fabricate high-quality ordered mesoporous solids with a variety of compositions and topologies, with some important and interesting works highlighted. These include the selection of surfactants on the basis of basic characteristics, mesophase behaviors, and inorganic and/or organic additives. The effects of synthetic parameters are summarized, such as hydrothermal and evaporation induced

Dongyuan Zhao

Dongyuan Zhao received his BS and MS in chemistry from Jilin University. He obtained his PhD in 1990 from Jilin University and Dalian Institute Chemical Physics. In 1992–1993, he was a visiting scholar at the Department of Chemistry, University of Regina and later carried out his postdoctoral research at the Weizmann Institute of Science (1993–1994), University of Houston (1995–1996), and University of California at Santa Barbara (1996–1998). He is now a Professor (Cheung Kong Professorship) in the Department of Chemistry at Fudan University. His current research interests include synthesis, structural characterization and application on ordered porous materials, such as mesoporous materials, zeolites, and coordination polymers.

self-assembly (EISA) conditions. The synthetic pathways and related mechanisms are introduced with some emphasis on EISA strategy. Design on the microscale (atoms and molecules) applies to many compositions, such as silicates, organosilicas, metals, sulfides, metal oxides, polymers, carbons, hybrid polymer–silica and carbon–silica nanocomposites, while design on the mesoscale is mainly on mesostructures, such as ordered two-dimensional (2D), ordered 3D, disordered and other mesostructures. Potential applications of mesoporous solids, particularly in optical devices, electrodes and biomaterials are also presented.

2 Design and synthesis of mesoporous solids

2.1 Nonionic surfactants

The main classes of nonionic surfactants for synthesizing ordered mesostructures are oligomeric alkyl ethylene oxides, oligomeric alkylphenol ethylene oxides, sorbitan ester surfactants and amphiphilic block copolymers. Commercial nonionic surfactants are frequently used and are listed in Fig. 1. In industry, they are usually utilized as detergents, emulsifiers, foamers, wetters, gel foaming agents, *etc*. To select a surfactant, its basic nature may give a guidance such as hydrophilic/hydrophobic ratio, critical micelle concentration (CMC), hydrophile–lipophile balance (HLB), critical micelle temperature (CMT), cloud-point (CP) value, *etc.*

Commercially available triblock copolymers from BASF Co. are listed in Fig. 2. The grid profiles of respective triblock copolymers with various molecular weight ranges of the hydrophobe are plotted as a function of the percentage of hydrophile in the block copolymers. Block copolymers with certain hydrophilic/hydrophobic ratios (for example, the top right corner area in Fig. 2) are extremely suitable for assembling ordered mesoporous silicates. Reversed PPO-PEO-PPO copolymers are seldom used in the synthesis of ordered mesoporous silicas, caused by the difficulty in the formation of oil-in-water micelles,[32] and they easily form reversed micelles. On the basis of the enormous studies on block copolymers, key to the use of reverse triblock copolymers for the fabrication of ordered mesoporous materials is their solubility in water, and an optimal balance between the hydrophobic and the hydrophilic portions.

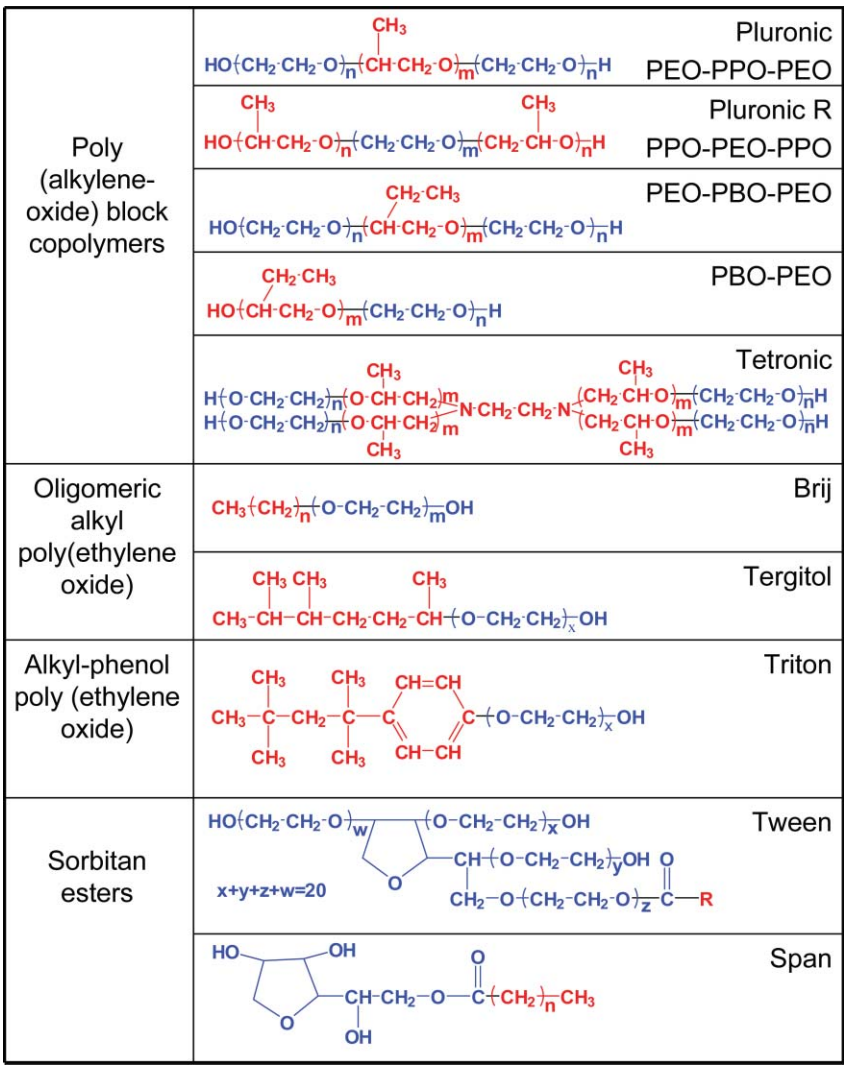

Fig. 1 Classical commercial nonionic surfactants.

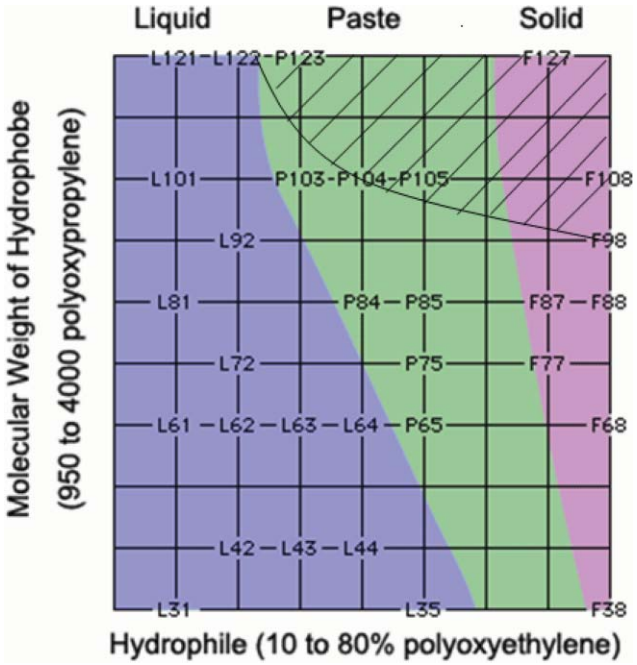

Fig. 2 Molecular weight ranges of the hydrophobe *vs.* the percentage of hydrophile of the block copolymer, reprinted with permission from http://www.basf.com/performancechemical/bcperfpluronic_grid.html

Table 1 Relationship between the CMC value of surfactant and the final mesostructure

CMC/mg L^{-1}	0	20	300
Formation of mesostructure	I	II	III

Otherwise, irregular aggregates will occur or precipitation will appear.[33] At the given PPO block length, an increase in the PEO block stabilizes the cubic and the hexagonal phases.[34] Therefore, the use of reversed triblock copolymers with long PEO chains may give rise to novel mesostructures.

Table 1 summaries a brief description of how CMC values of surfactants affect final mesostructures in aqueous media.[35] In general, if surfactants are located in region I, ordered mesostructures are always obtained. In region II, strategies can be used to decrease the CMC values to yield ordered mesostructures. Surfactants with large CMC values generally give cubic mesostructures. It is difficult to make ordered mesostructures when CMC values of surfactants are higher than 300 mg L^{-1}. Namely, low CMC values of surfactants are an important criterion towards increasing regularity of mesostructures.

Based on emulsification data, semi-empirical HLB numbers, ranging from 0 to 40, can be assigned to surfactants which have a hydrophilic–lipophilic balance. Surfactants with HLB values ranging from 4 to 12 favor the formation of ordered mesostructures. If HLB values of surfactants are higher than 12, cubic and disordered mesostructures are the possible products with these templates, and the syntheses are difficult to control. Lyophilic surfactants with HLB values lower than 4 always direct the formation of lamellar mesostructures.[36]

The surfactant micelles are influenced by many factors, such as temperature, concentration, inorganic salts, organic agents, pH values, *etc*. These characteristics, together with sol–gel chemistry of inorganic solids guide the synthesis, which will be discussed in the following sections.

The successful syntheses of a new family of mesoporous silica materials (such as SBA-15) were carried out by using nonionic alkyl PEO oligomeric surfactants, diblock copolymers, triblock copolymers and star copolymers as templates under acidic aqueous media. A large number of highly ordered mesoporous silica materials with various pore packing symmetries and well defined pore connectivities have been prepared.[5,36]

Similar to nonionic surfactants, long-chain alkyl amines, such as primary alkylamines (dodecylamine and hexadecylamine) and *N*,*N*-dimethylalkylamines (*N*,*N*-dimethyldodecylamine and *N*,*N*-dimethylhexadecylamine) have amiphiphilic nature. However, only worm-like mesostructures can be obtained due to their poor water-solubility in neutral media.[9,37] Alkylamines can be protonated under acidic conditions and their solubility is improved, and the interaction with inorganic precursors is enhanced. Highly ordered mesoporous silicate materials can therefore be easily obtained similar to those cases templated by cationic surfactants.[38]

Lab-made surfactants are adopted to expand the pores of mesoporous silicates or to implant functional groups inside mesochannels, which can be applied into large-molecule involved processes and heterostructure devices, respectively.[12,39–47] By employing PI-*b*-PEO, poly(isobutylene)-*block*-poly(ethylene oxide) (PIB-*b*-PEO) and poly(styrene)-*block*-poly(ethylene oxide) (PS-*b*-PEO) diblock copolymers, large-unit mesostructured silicates have been templated.[12,39–44] The use of block copolymers with high molecular weight is suggested as an easy pathway for the preparation of various silica-type mesostructures that extends the accessible length scale by about an order of magnitude. However, the expected large mesopore sizes are not observed in some cases. N_2 adsorption measurements show the BET (Brunauer–Emmett–Teller) surface areas are near zero. This is probably due to the isolated spheres packing model which results in thick pore walls and no micropore connections between mesopores.[42–44] Brinker and co-workers fabricated photoluminescent silica composites by using amphiphilic surfactants containing diacetylene, pyrrole or thiophene as SDAs.[45,48] The functional surfactants also include amphiphilic poly(phenylene ethynylene) (PPE) and block copolymer hexyl-oligo(*p*-phenyleneethynylene)-poly(ethylene oxide) (Hex-OPE-PEO).[46,47]

2.2 Mesophase instruction

The hydrophilic/hydrophobic volume ratio (V_H/V_L) is suggested especially for nonionic-surfactant-templating systems to account for the formation of different mesophases.[49] Table 2 classifies the typical ordered mesostructured silicates synthesized with nonionic surfactants.

Nonionic surfactants with high V_H/V_L ratios (such as F108, F98 ($EO_{123}PO_{47}EO_{123}$), F127 and Brij700 ($C_{18}H_{37}EO_{100}$)) favor the formation of caged-like cubic mesoporous materials, whose topological curvatures are rather high, while block copolymers with medium hydrophilic/hydrophobic ratios

Table 2 List of typical ordered mesoporous silicate materials templated by nonionic surfactants

Structure-directing agent	Researchers or material	Mesostructure (space group)	Remarks	Ref.
$C_{12}EO_8$, $C_{16}EO_8$	Attard and co-workers	*p6m*	LCT mechanism, small pore	11
Brij 56 $C_{16}EO_{10}$	SBA-11	$Pm\bar{3}m$		36
	CMI-1	*p6m*		50
Brij 76 $C_{18}EO_{10}$	SBA-12	$P6_3/mmc$	Mixed hcp and ccp phases	36
Brij 700 $C_{18}EO_{100}$	ST-SBA-16	$Im\bar{3}m$	Small pores, thick walls	51
P123 $EO_{20}PO_{70}EO_{20}$	SBA-15	*p6m*	Highly ordered large pores	5,36
	MSU-H	*p6m*	Neutral pH	52
	IBN-4	*p6m*	With FC-4, nanoparticles	53
	JLU-20	*p6m*	With FC-4, high hydrothermal stability	54
	FDU-5	$Ia\bar{3}d$	Acidic synthesis, with MPTMS, EISA	55
	Flodstrom *et al.*	$Ia\bar{3}d$	With inorganic salts	56
	KIT-6	$Ia\bar{3}d$	With butanol, low acid concentration	57,58
	Schuth and co-workers	$Ia\bar{3}d$	With VTES and inorganic salts	59
	Che *et al.*	$Ia\bar{3}d$	With MPTMS	60
	FDU-5	$Ia\bar{3}d$	Post-solvothermal synthesis	61
	Chen *et al.*	$Ia\bar{3}d$	With SDS	62
F127 $EO_{106}PO_{70}EO_{10}$	FDU-12	$Fm\bar{3}m$	ultra-large caged	63
	KIT-5	$Fm\bar{3}m$	With butanol, low acid concentration	64
	Chen *et al.*	$Fm\bar{3}m$		65
	IBN-2	$Fm\bar{3}m$	With FC-4 and TMB, mixed hcp and ccp phases	53
	SBA-16	$Im\bar{3}m$		36
	IBN-1	$Im\bar{3}m$	With FC-4 additive	53
	Chen *et al.*	$Im\bar{3}m$	With AOT	65
	Feng *et al.*	*p6m*	Monolith, with organic additives	66
	Chen *et al.*	*p6m*	With AOT	65
	Chen *et al.*	$Ia\bar{3}d$	With AOT and TMB	65
F108 $EO_{132}PO_{50}EO_{132}$	Yu *et al.*	$Im\bar{3}m$	Highly ordered crystals	67
B50-6600 $EO_{39}BO_{47}EO_{39}$	Jaroniec and co-workers	$Fm\bar{3}m$	Mixed hcp and ccp phases large-caged	68
	FDU-1	$Im\bar{3}m$	Large-caged	69
PI-*b*-PEO poly(isoprene)-*block*-poly(ethylene oxide)	Wiesner and co-workers	$Im\bar{3}m$	''The plumber's nightmare''	39–41
Vitamin E TPGS 1000 $C_{33}O_5H_{54}(CH_2CH_2O)_{23}$	DAM-1	*p6m*		70
d_8PS-*b*-P2VP poly(d_8-styrene-*block*- poly(2-vinylpyridine)	Kramer and co-workers	*p6m*	Thin film, with low to moderate cross-linking degree of d_8PS-*b*-P2VP	71
$EO_{17}MA_{23}$ poly(ethylene oxide)- -poly(methyl acrylate)	Chan *et al.*	$Ia\bar{3}d$		72
PI-*b*-PMDSS-*b*-PI poly(isoprene)-*block*-poly(pentamethyldisilylstyrene)-*block*-poly(isoprene)	Chan *et al.*	$Ia\bar{3}d$	Silicon-containing triblock copolymer	73

(*e.g.* P123 and B50-1500 ($BO_{10}EO_{16}$, BO = butylene oxide)) usually direct the synthesis of mesostructures with medium curvatures (*e.g.* 2D hexagonal structure with space group of *p6m* or 3D bicontinuous cubic $Ia\bar{3}d$).[36] The concentration of block copolymers which affect the V_H/V_L ratios can also alter mesostructures. Normally higher concentrations lead to mesostructures with lower mesophase curvature[74,75] and is especially suited for the rational synthesis of mesoporous solids *via* the ''true'' liquid-crystal templating (LCT) pathway.

2.3 Additives

2.3.1 Mixed surfactants. Owing to the unique aggregation behaviors, mixed-surfactant systems share many advantages over single-surfactant systems, such as variation in CMT and CMC values, adjusting interactions with inorganic silica species, tuning pore sizes, getting hierarchical pore structures and causing phase transformations, *etc*.

The surfactants should be compatible to obtain ordered mesostructures. During the hydrothermal synthesis process, the uniform micelles are important for controlling the uniform surface curvature.[76,77] Co-templates of triblock copolymers and alkyl polyethylene oxides were found to increase the efficiency of cooperative assembly of organic and inorganic species and lead to the formation of highly ordered silica mesostructures.[75]

The ability of cationic or anionic surfactants to incorporate special characteristics into nonionic-surfactant-templating systems has enabled a range of achievements. The first one is establishing diverse pore architectures. From a general thermodynamic point of view, the creation of hierarchical micellar systems is usually unfavorable.[78] Mixing most cationic surfactants, that can template small mesopores, and block copolymers, whose products are large-mesopore in nature, may result in either phase separation or compound micelles which favor the formation of uniform large mesopores. Consequently, the special properties of surfactants themselves should be considered. Ionic liquids and small fluorinated co-templates are used in triblock-copolymer-templating systems to create bimodal mesoporous materials.[78–80] For example, Smarsly and co-workers reported the ionic liquid 1-hexadecyl-3-methylimidazolium chloride (C_{16}minCl) exhibits an advantageous templating role, with small mesopores (2–3 nm) being located between block copolymer mesopores,[79]

while phase separation occurs in the binary surfactant system of cetyltrimethylammonium bromide ($C_{16}H_{33}N(CH_3)_3Br$, CTAB) and PS-*b*-PEO. The second advantage is the synthesis of mesostructured nanoparticles. By utilizing different interaction mechanisms between cationic and nonionic surfactants and silicates, Imai and co-workers obtained silica nanoparticles with ordered mesostructures.[81] Han and Ying reported a distinct confined-growth effect of cationic fluorocarbon surfactants such as FC-4 ($C_3F_7O(CFCF_3CF_2O)_2CFCF_3$-$CONH(CH_2)_3N(C_2H_5)_2CH_3I$), which can not be used as SDAs for mesoporous materials, on the formation of triblock-copolymer-templating ultrafine mesostructured particles.[53] In addition, cationic fluorocarbon and hydrocarbon polymer surfactants were used as an example for illustrating the synthesis of stable, ordered mesoporous silica-based materials through a high-temperature hydrothermal process.[54] Blending surfactants have been also used to demonstrate how V_H/V_L ratios affect mesostructures. Cubic bicontinuous $Ia\bar{3}d$ mesostructures can be easily templated by mixed surfactants such as cationic and nonionic alkyl PEO surfactants, as well as triblock copolymer P123 and anionic sodium dodecyl sulfate (SDS) surfactant.[62,82] The addition of anionic surfactant such as sodium dioctyl sulfonate (AOT) and organic swelling agent 1,3,5-trimethylbenzene (TMB) into the triblock copolymer F127 assembly system causes the expansion of hydrophobic volumes and hence the phase transformation.[65] The transformation of the highly ordered mesostructures from face-centered cubic (space group $Fm\bar{3}m$) to body-centered $Im\bar{3}m$ then towards 2D hexagonal *p6m* and eventually to cubic bicontinuous $Ia\bar{3}d$ symmetries has been achieved by tuning the amount of AOT and TMB (Fig. 3).

2.3.2 Inorganic additives. The addition of inorganic salts (electrolytes) significantly affects CMC values of surfactants. The energy required to create volume accommodating hydrophobic solute is changed in an electrolyte solution due to water–ion interactions. Such a variation can be attributed to *"salting in"* or *"salting out"* effects.

If energy required is increased by adding electrolytes, a *"salting out"* effect occurs. Micellization is favored and the CMC decreases. In practice, highly hydrophilic block copolymers (*e.g.* F127, F108, F98 and Brij 700) are ideal SDAs for the formation of caged mesoporous materials from the viewpoint of their intrinsic packing symmetries and mesophase behaviors, although it is somewhat difficult to prepare ordered mesostructured solids. Fortunately, this conflict can be overcome when *"salting out"* inorganic salts (such as, NaCl, KCl, K_2SO_4, Na_2SO_4) are added into the synthetic batches.[67,83] In addition, this effect can be utilized to lower the CMC and CMT values of block copolymers. The synthesis can be accelerated and improved by the addition of inorganic salts. Simultaneously, highly ordered mesoporous silicates can be prepared with low block copolymer concentrations or at low temperatures, even at 10 °C for the case of P123-templating SBA-15.[84]

The effects of inorganic salts on ionic surfactants depend on the radii of hydrated anions and cations, and are substantial for small hydrated ions. The Hofmeister series of anions explain well the self-assembly and phase behaviors of cationic surfactants.[85–87] However, anions also affect nonionic surfactants in significant ways. Some other factors, such as the solubility of nonionic containing ether groups which decreases upon dehydration should be considered.[85,88] Tang *et al.*[88]

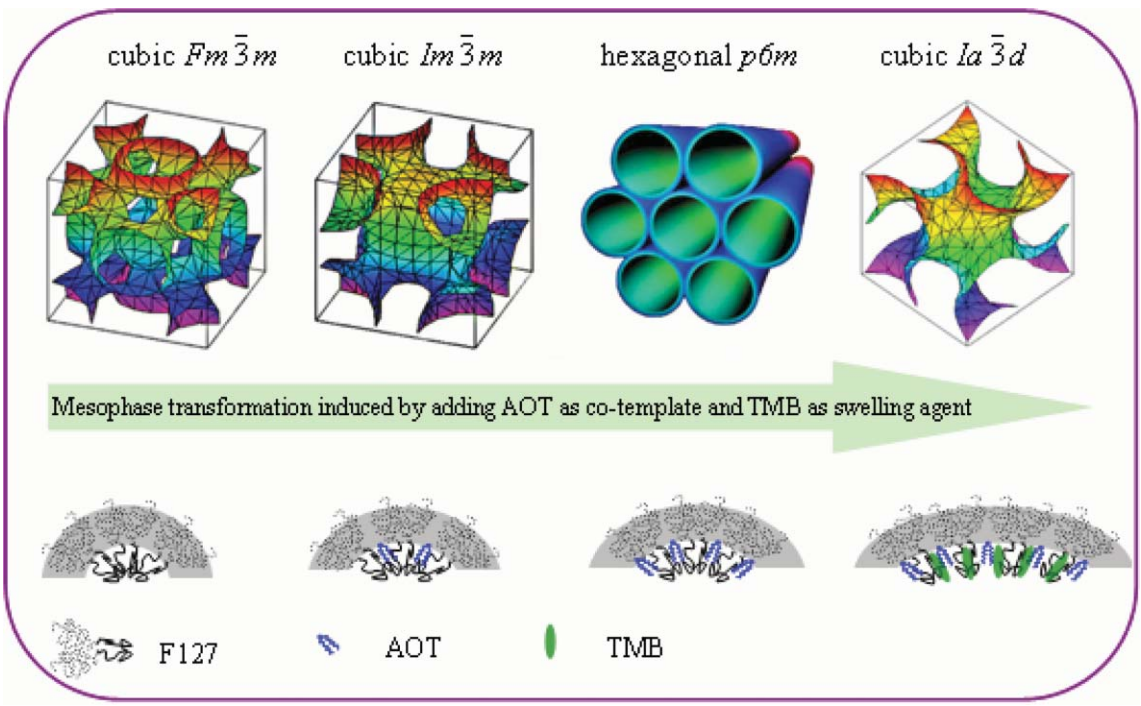

Fig. 3 Schematic representation of the mesophase transformation induced by co-template AOT and swelling agent TMB in the amphiphilic triblock copolymer F127 assembly system. With the increase of anionic surfactant AOT and/or organic additive TMB concentration, the interface curvature of F127-AOT mixed micelles is reduced, resulting in the mesophase transformation from cubic close packing (face-centered structure) to loose packing (body-centered bicontinuous structure). Reprinted with permission from ref. 65. Copyright 2006, Royal Society of Chemistry.

found an order of SO_4^{2-} (HSO_4^-) > NO_3^- > Cl^- in acidic solution to cause the transformation from *p6m* to $Ia\bar{3}d$ mesostructure when triblock copolymer P123 is employed as a template. This order is different from either the Hofmeister series or the reverse, which can be attributed to the balance between dehydration and radii effects.

By contrast, *"salting in"* inorganic salts increase CMC values, and can sometimes increase the mesophase curvature, as has been demonstrated by Flodstrom *et al.*[56] They used the inorganic additive NaI to tune the mesophase from basically multi-lamellar vesicles to cubic bicontinuous ($Ia\bar{3}d$) structure, which is situated between lamellar and 2D hexagonal phases.

Inorganic salts play a vital role on the morphologies of mesoporous silicates. A novel mesoporous silica membrane with 3D sponge-like macrostructures were reported by Stucky and co-workers.[89] The macropore dimensions were established by the sizes of droplets of aqueous electrolytes, such as NaCl, LiCl, KCl, NH_4Cl or $MgSO_4$. Adding inorganic salts in triblock copolymer systems can yield large-pore, mesostructured SBA-16 spheres with macroscopic sizes of about several millimeters.[90] Yu *et al.*[67] have demonstrated the synthesis of cubic mesoporous silica ($Im\bar{3}m$) with uniform rhombodecahedral shape under acidic conditions by using commercial nonionic block copolymers as templates and inorganic salts as additives (Fig. 4).

Inorganic salts can significantly facilitate the formation of highly ordered mesoporous organosilicas,[91,92] which will not be detailed herein.

Some inorganic substances which can be "dissolved" in the micelles can expand pore diameters. During the hydrolysis process of silicate, supercritical (sc) CO_2 can act as a swelling agent to tailor the pore sizes of hexagonal mesoporous silicas.[93] Substantial swelling effects were found for mesoporous silicas templated by triblock copolymers, such as P123, F127 and P85. Somorjai and co-workers found the preexistence of a certain concentration of metallic nanoparticles can expand the mesochannels of SBA-15 when P123 is used as a template.[94]

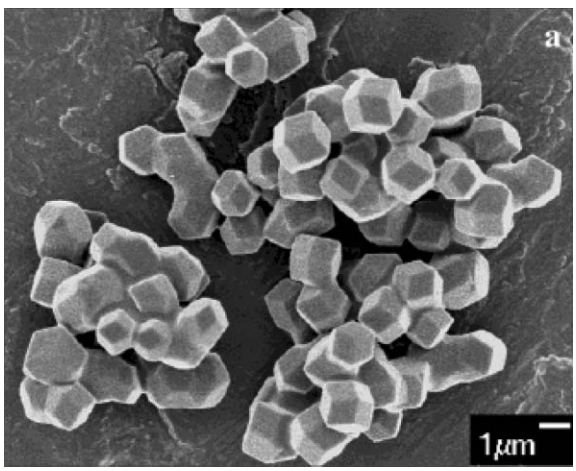

Fig. 4 SEM images of mesoporous single crystals synthesized templated by F108 with 0.5 mol L^{-1} K_2SO_4, reprinted with permission from ref. 67. Copyright 2002, American Chemical Society.

2.3.3 Organic agents. Various organic additives, such as TMB, alcohols (*e.g.* butanol, heptanol, hexanol), alkanes (*e.g.* hexane, heptane, octane, nonane, decane, dodecane, pentadecane, heptadecane and nonadecane) and *N*,*N*-dimethylformamide (DMF), have been added to acidic cooperatively assembling systems.

Solubilization of impurities in micelles causes changes in the surface energy. Lyophilic organics can aid or oppose the formation of micelles. Some organic additives adsorb within micelles and reduce CMC values. Small molecules favor location near the micelle–water interface while large molecules adsorb in the core. The micellar shapes are therefore different, causing phase transformation or mesopore enlargement.[51,55,57–60,63,95–100] The morphologies of final products can also be affected.[66,101–105] These additives are effective at low concentrations. At high concentrations, agents such as dioxane, short-chain alcohols and ethylene glycol can enhance the solubility of monomeric surfactants, thus suppressing micellization and raising CMC values of nonionic surfactants.

In the presence of 3-mercapropropyltrimethoxysilane (MPTMS) or organic molecules, *e.g.* toluene, benzene, xylene, TMB, *etc*, cubic bicontinuous $Ia\bar{3}d$ mesoporous silica with large pore size was templated by Pluronic P123 under acidic conditions.[55] The deceased V_H/V_L ratio results in a transition of the mesostructure from high-curvature hexagonal *p6m* to a low-curvature cubic bicontinuous $Ia\bar{3}d$ mesostructure.[55,60] Later on, large-pore $Ia\bar{3}d$ mesostructures were also reported by adding vinyltriethoxysilane (VTES) and inorganic salts, and $(PPh_2)Si(OEt_3)_3$ into acidic P123-templating systems.[59,95] The expansion behavior of *n*-butanol with triblock copolymers favors the formation of mesoporous silica with cubic $Ia\bar{3}d$ structure in weakly acidic solution.[57]

The addition of TMB can improve ordering of mesostructures in the case of highly hydrophilic SDAs, *e.g.* Brij 700 and F127.[51,63]

When hydrophobic organic species are soluble inside the hydrophobic regions of surfactant micelles, they lead to a swelling of the micelles and in turn, the enlargement of pore sizes of mesoporous solids.[96] To evaluate the swelling role, the solubility of organic additives in surfactant micelles should be considered[96] and large organic hydrocarbons such as decane, isopropylbenzene and TMB are efficient in this context.[97–99] With the aid of TMB molecules, the pore sizes of mesoporous silicates can be enlarged to 40 nm in acidic triblock copolymer-templating systems.[97] The mesostructures are however, disordered. By adding TMB as a swelling agent, the pore size can only increase to 20 nm for SBA-15 with the maintenance of an ordered mesostructure. Use of a large amount of TMB in the synthesis system of SBA-15 leads to a siliceous mesocellular foam (MCF).[97] The pore size of highly ordered 2D hexagonal mesoporous silica can reach 11 nm in the presence of F127, AOT and TMB.[65] Assisted by TMB and KCl, an exceptionally large pore size (~27 nm) of face-centered cubic mesoporous silica FDU-12 (space group $Fm\bar{3}m$) results in a F127-templating system when the synthesis temperature is lowered to 15 °C.[100]

A general method for the synthesis of periodic mesostructured silicate monoliths was reported by Feng *et al.*[66] *via* a

direct LCT mechanism in multicomponent (tetramethoxysilane (TMOS), surfactants and alcohol) systems. Similarly to this route, 3D mesoporous silica materials (HOM-*n*) can be prepared by the addition of alkanes with variable chain lengths into the lyotropic liquid crystal phases of Brij56 and Brij76.[101,102] An emulsion of triblock copolymer F68 ($EO_{76}PO_{29}EO_{76}$), TMB and sodium silicate gives rise to hollow silica spheres.[103] To yield transparent and crack-free mesostructured silica monoliths, Yang *et al.*[104] demonstrated a liquid-paraffin-medium protected solvent evaporation method by using triblock copolymers as templates. The coverage of paraffin on freshly dried monoliths significantly reduces the original surface tension of the bare monoliths, and thereby shortens the traditional solvent evaporation process of silica gels to get ordered silica monoliths. Zhao and co-workers prepared doughnut-like SBA-15 with ordered curve mesochannels, using DMF as the co-solvent.[105]

2.4 Hydrothermal synthesis

The synthesis of mesoporous materials is generally performed *via* a solution reaction. Water is the most common solvent and medium. In a hydrothermal process, several parameters influence the resultant products, such as concentration of surfactants, synthesis (solution reaction) temperature, acidity, hydrothermally treated temperature and time, *etc.* which affect the degree of hydrolysis and cross-linking of the silicates.

Higher ordered mesostructures can be derived with lower surfactant concentration, which could be attributed to the slower assembly of mesostructures.[14] However, normally the concentration should be higher than the CMC value of the surfactant. As mentioned above, the surfactant concentration also affects the final mesostructure and is obviously related to the surfactant phase behavior to some extent.[106] The phase diagram is an efficient, broadly applicable instrument for determining synthesis and mesostructures. However, the formation of mesophases does not exactly follow such reported diagrams, because the hydrophobic/hydrophilic property of a given system is continuously changed during the polymerization of inorganic species.

The synthesis temperature for mesoporous materials is relatively low, ranging from −10 to 130 °C, but it is normally higher than room temperature owing to the high CMT values. Many nonionic surfactants show the problem that they become insoluble in warm water. This temperature is known as the cloud-point (CP), where the solution becomes cloudy due to phase separation and the surfactant begins to precipitate. The synthesis temperature must be lower than the CP values of surfactants. In the synthesis of SBA-15 templated by triblock copolymer P123, the optimal synthetic temperature is 35–40 °C. Either lower or higher temperature may prevent the formation of micelles due to the solubility limit and CMT value.[5,36,107] The CMC and CP values are influenced by many factors, such as solvents, co-surfactants, inorganic salts and organic agents, which have been and will be discussed in separate sections.

The synthesis temperature is high using block copolymers with high CMT and CP values. It is found that ordered mesoporous silicates can only be obtained at temperatures higher than 90 °C in the P65 ($EO_{20}PO_{30}EO_{20}$) and P85 ($EO_{26}PO_{39}EO_{20}$) systems, both of which have CP values of 82 °C in water.[108]

Why is the synthesis temperature in P65 and P85 systems higher than their CP values in water? This can be explained by the fact that CP values differ in various media. The CP values of surfactants are increased in strongly acidic solutions with ethanol that is generated by the hydrolysis of TEOS. In the presence of 2 M HCl and ethanol, the CP values of P65 and P85 are higher than 95 °C. It is thus reasonable that mesoporous materials can be synthesized at 95 °C.[108] However, it is often desirable to decrease the synthesis temperature which reduces the reaction rate and thereby improves the crystalline regularity.

The assembly of inorganic and organic periodic composite materials appears to occur by a double-layer hydrogen bonding ($S^0H^+)X^-I^+$ pathway by reason of the assembly characteristics of PEO type nonionic surfactants. On the other hand, the condensation rate of silicate species under neutral conditions (pH = 7) is too fast to be controlled. As a result, most efficient syntheses of ordered mesoporous silica structures are carried out in acidic media. Only a few strategies have been proposed to prepare ordered periodic mesoporous silica structures under neutral or alkaline conditions. An example is ordered hexagonal MSU-H by using sodium silicate as the silicate source and triblock copolymer P123 as the SDA in near-neutral media.[52] Voegtlin *et al.*[109] employed nonionic oligomeric surfactants as SDAs to synthesize mesoporous silica under near-neutral conditions in the presence of fluoride ions. Utilizing fluorides as a catalyst or co-catalyst to control the rates of hydrolysis and condensation of TMOS, Stucky and co-workers have developed a one-step synthesis of ordered hexagonal silica-surfactant mesostructured composites under such conditions with a wide range of pH values (pH = 0–9).[110]

By lowering the pH values of solution, the synthesis rate can be accelerated. The optimum pH value is <1 when HCl is used as an acidic catalyst. A higher acid concentration results in a faster precipitation rate. However, a solution containing a high concentration HCl (>4 M) always produces low-quality materials. Besides HCl, HNO_3, HBr, HI and H_2SO_4 can serve as acid catalysts. Weak acids, such as H_3PO_4 and acetate acid, are rarely adopted due to the low quality products obtained. It is unknown whether the products contain phosphorus in H_3PO_4-containing systems because phosphates may cross-link with silicates.

Since the EO moieties of block copolymers are readily protonated in strongly acidic media, the higher the concentration of H^+ , generally the more hydrophilic the block copolymer. This provides us a way to slightly tune the inorganic/organic biphasic interplay in aqueous media. As shown in Fig. 5, high-quality 3D cubic SBA-16 ($Im\bar{3}m$) mesostructure can be obtained within a rather large synthetic composition range in a solution with low acid concentration (0.5 M HCl) which is believed to be synthesized with difficultly in 2 M HCl solution.[111,112] Bicontinuous cubic ($Ia\bar{3}d$) and face-centered cubic ($Fm\bar{3}m$) silicate mesostructures can also be successfully obtained in this media with different SDAs.[58,64] This is explained by that the low-concentration acid catalyst favors slow condensation kinetics of silicate species. The preparation

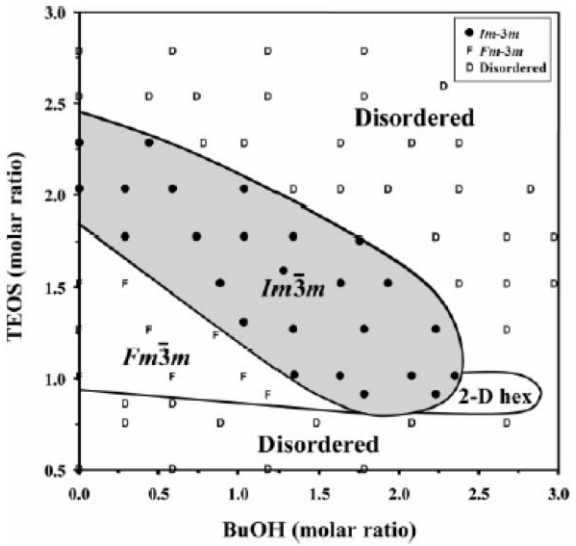

Fig. 5 Diagram of mesophase structures established according to X-ray diffraction (XRD) measurements. Each sample is prepared with a molar ratio of 0.0035 F127 : *x* TEOS : *y* BuOH : 0.91 HCl : 117 H_2O. Reprinted with permission from ref. 112. Copyright 2006, American Chemical Society.

of mesoporous silicates is almost thermodynamically controlled with the addition of *n*-butanol.

When the pH value is in the range from 1 to 2, the precipitation of mesoporous silicates is extremely slow, probably corresponding to the isoelectric point of orthosilicic acid. The stable prehydrolyzed silica sol under a solution at pH = 2 makes detailed analysis possible, although syntheses have seldom been carried out under this condition. Taking advantage of this characteristic, Prouzet and co-workers investigated that the main components, *i.e.* soluble silica oligomers and nonionic surfactants micelles, show interactions at this stage.[25,113]

Hydrothermal treatment is adopted after the solution reaction. It is one of the most efficient methods to improve mesostructured regularity of products where the mesostructures undergo re-organization, growth and crystallization.[25,36] The synthesis temperature is generally lower than that for zeolites, ranging from 80 to 150 °C, in which the range 95–100 °C is mostly used. High-temperature would cause decreasing regularity and decomposition of surfactants which may result in the formation of microporous materials.[114]

A long synthesis time ranging from days to one month is necessary to obtain hydrothermally treated mesoporous solids with the range 1–7 days being considered efficient. Hydrothermal treatment times can be shortened to 2 h or even shorter when microwaves are employed.[115] The hydrolysis and cross-linkage of inorganic species and assembly further proceeds during the hydrothermal process. The adsorption and structural properties of mesoporous silicates SBA-15 and SBA-16 can thus be tailored to some extent by adjusting the hydrothermal temperature and time.[116,117] A larger pore size is always produced at higher temperatures and longer hydrothermal treatment times. As shown in Fig. 6, the mesopore sizes of SBA-15 can be easily tuned from 9.5 to 11.4 nm and from 4.6 to 10 nm by prolonging the hydrothermal synthesis time from 6 h to 4 days and increasing the hydrothermal temperature from 60 to 130 °C, respectively.[116,117] Increasing the hydrothermal temperature and time for SBA-16 from 45 °C and 1 day to 100 °C and 2 days thins the pore walls, reduces intra-wall micropores and creates large primary mesopores. Pore sizes of mesoporous silicas with $Ia\bar{3}d$ symmetry were tuned from 4 to 10 nm when the hydrothermal temperature was increased from 65 to 130 °C.[58]

2.5 Non-aqueous synthesis

Non-aqueous synthesis provides unique advantages in the convenient synthesis of ordered mesoporous materials, specifically for mesoporous thin films, membranes, monoliths and spheres. A dominant strategy is to template the mesophase growth by volatile solvent evaporating induction, known as the EISA strategy.[17] It was first used by Brinker and co-workers in the preparation of mesoporous silica thin films. Stucky and co-workers further developed this method to synthesize large-pore mesoporous solids.[18,74]

In the case of fabricating mesostructured silica films, TEOS was dissolved in the organic solvent and pre-hydrolyzed with a stoichiometric quantity of water (catalyzed by acids, such as HCl) at a temperature of 25–70 °C. Low-polymerized silicate

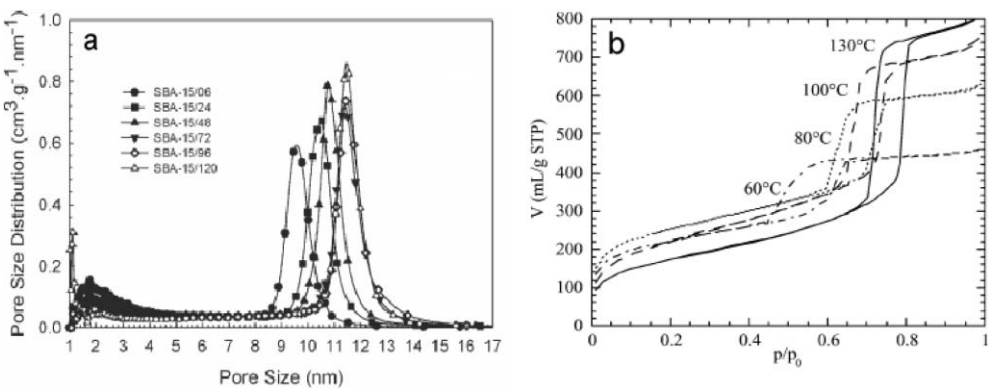

Fig. 6 (a) Pore size distribution curves for SBA-15 hydrothermally treated at 100 °C for 6, 24, 48, 72, 96 and 120 h. (b) Nitrogen sorption isotherms for SBA-15 hydrothermally treated at 60, 80, 100 and 130 °C. Reprinted with permission from ref. 116 and 117. Copyright 2003, Royal Society of Chemistry and copyright 2003, Royal Society of Chemistry and The Centre National de la Recherche Scientifique.

species can randomly interact with surfactants. Then silicate species polymerize and condense around surfactants with the evaporation of solvent which is improved by the gradually condensed acid. Surfactant-templating assembly occurs accompanied with the concentrated surfactant solution, forming ordered mesostructures. This process exhibits an extremely fast formation rate of the mesostructure, only in several seconds. Therefore, the mesophase transformation is rarely observed.[74]

An important feature of the EISA strategy is a wide range of SDAs that can be employed. For example, triblock copolymers F108 and F98 are very difficult to template the formation of mesostructures under aqueous conditions, while this occurs much more easily *via* EISA. This strategy is also confirmed to be easy and convenient to obtain the 3D cubic silica mesophase ($Im\bar{3}m$). By using block copolymers with large EO segments, *e.g.* F127, F108, F98 and mixed surfactants, the cubic SBA-16 mesostructure can be easily synthesized.[75]

Typical solvents are weakly polar and few syntheses adopt non-polar and oily solvents. Silica nanowires with adjustable diameters were prepared with P123 or F127 by the EISA approach in toluene and xylene solutions. The formation of this type of arrays is related to the reversed mesophase of surfactants in oily solvents. Tuning the ratio of oil/water can give rise to hollow sphere silica.[118] The synthetic conditions are quite strict, with silica mesostructures, reversed mesostructures and their mixtures being possible products. The possible reasons are that a little water is incorporated in the process upon oily solvent evaporation and the reversed micelles revert to their normal form.

XRD patterns display relatively wide diffraction peaks of the samples made by EISA at 2θ of 3–5°. Their mesostructures are seemingly less ordered. However, transmission electron microscope (TEM) images reveal large domain ordering and the ordered arrays are uniformly observed. The lack of XRD diffraction peaks could be ascribed to the extremely fast formation rate of mesostructures that cause nonuniform micelles. Certain substrates are normally required for controlled deposition of samples. This imposes a strain field and generates a uniaxial lattice distortion. Qualitative and quantitative analysis can be made on this distortion and show the relation with lowering the mesostructure symmetry.[61,119–121]

Nitrogen adsorption isotherms reveal that mesoporous materials from the EISA strategy generally have lower surface areas than those prepared by the hydrothermal synthesis method. This has not been fully understood up to now, but can be predicted as arising from lack of microporosity.[43,74] This phenomenon may be caused by either the reduced inclusion of EO segments into the inorganic frameworks or the retraction of EO chains under the faster self-assembly conditions.[61,122] Non-aqueous solvents may inhibit the charge coupling or other interplay between the inorganic species and the hydrophilic corona. Formation of dense inorganic frameworks may be another reason. With the same conditions of synthetic temperature and triblock copolymer P123 template, SBA-15 mesoporous silica synthesized *via* the EISA strategy has much larger pore size (9.0 nm) than that (4.6 nm) from hydrothermal precipitation at relative low temperature (60 °C).

2.6 Re-crystallization

Re-crystallization is an efficient method of enhancing mesostructural regularity by treating as-synthesized powder samples (for most cases, silicates) without washing in deionized water at 100 °C for several days (about 1 week). The advantages are improved quality (regularity, thermal stability, *etc.*) and in some cases enlargement of pore sizes.[123] This process is quite complicated. Dissolution and crystallization of silicate species and re-organization of mesostructures may occur. This is different from hydrothermal treatment despite seeming similarity. By comparison, the re-organization rate in re-crystallization may be slower and more localized due to separated surfactants and unreacted silicate species. Here unwashed samples are favorable, because residues of acid or base catalysts, silicate oligomers, and surfactants make the re-organization of mesostructures feasible. Mesoporous silica thick membranes templated by P123 from the EISA approach show improved regularity after re-crystallization at 100 °C for 3 days, as evidenced by at least three well-resolved XRD peaks. The resultant material has a highly ordered 2D hexagonal mesostructure with high surface area (840 $m^2\ g^{-1}$), large pore size (9.0 nm) and large pore volume (1.12 $cm^3\ g^{-1}$).

Alternatively, organic solvents can be used in the re-crystallization. A solvothermal re-crystallization procedure was used for as-synthesized FDU-5 membranes which are flexible hybrids consisting of low polymerization degree inorganic silicate frameworks and relatively high content organic matrices.[61] This process causes a phase transformation from a 2D hexagonal to a 3D bicontinuous cubic FDU-5 mesostructure. To help visualize the possible structural correlation between the two mesostructures, a simplified schematic diagram is shown. In terms of equivalence of the cylinder axis (parallel to the (10) plane) of the hexagonal phase to the body diagonal (parallel to the (211) plane) of the gyroidal cubic phase, the rudimentary and final channel structures viewed from [10]h and [211]c directions are shown in Fig. 7(a) and (c), respectively. For the 2D hexagonal mesostructure, the channels A, B and C are equal. An intermediate state (Fig. 7(b)) caused by the thermally induced framework rearrangement, assumes that channel B begins contacting channel A and C at equidistant sites (note the adjacent A and C channels are always separated). A final form, *i.e.*, 3D bicontinuous cubic mesostructure, is achieved by uniformly dividing channel B and merging totally with channels A and C at the contacting sites, accompanying the curvature change. The simulated perspective model of interwoven channels (Fig. 7(d)) gives a further 3D insight into the planar structures shown in Fig. 7(c).

3 Design of synthesis pathway

The development of mesoporous materials must take into consideration the assembling modes and fabricating processes. Mobil scientists proposed a LCT mechanism. It is proved to be always ''true'', because the steps are roughly involved in almost all possibilities. Two main pathways are efficient to synthesize ordered mesostructures, the ''true'' LCT pathway and surfactant-templating assembly with inorganic oligomers or nanoparticles.

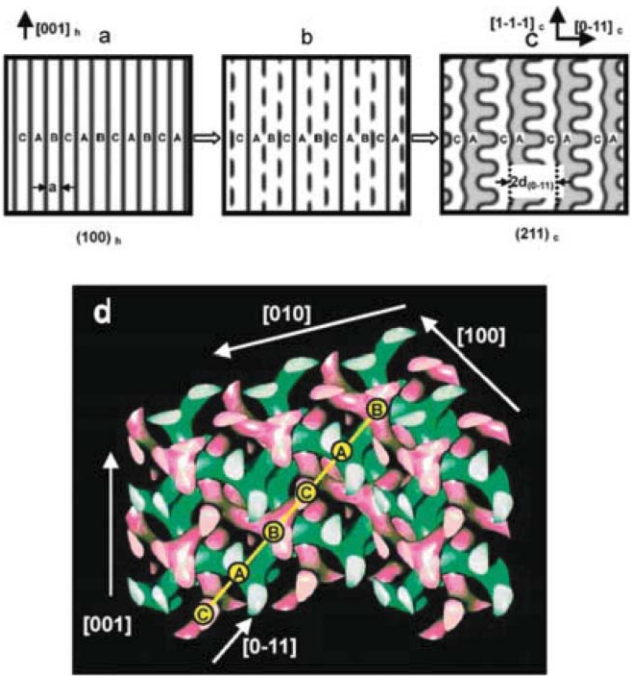

Fig. 7 Possible phase transition model from *p6m* to $Ia\bar{3}d$: (a) (100) plane of 2D hexagonal phase, (b) an intermediate phase, (c) (211) plane of cubic gyroidal phase, and (d) 3D model of double gyroidal channel structures. Reprinted with permission from ref. 61. Copyright 2004, American Chemical Society.

3.1 Liquid-crystal template pathway

The synthesis utilizes the true- or semi-liquid-crystal phase for surfactant-templating assembly to obtain ordered mesoporous solids. By using high-concentration nonionic surfactants as templates, Attard and co-workers synthesized mesoporous silicas.[11] Lyotropic liquid crystals provide an organized scaffold. Inorganic precursors grow around the surfactants. After the polymerization and condensation, the organic template can be removed, leaving a mesoporous material whose structure, pore size and symmetry are determined by the liquid-crystal scaffold.

The EISA strategy can also be assigned to this pathway.[17] It employs versatile solvent evaporation to induce the formation of mesostructures. Sanchez and co-workers have carried out elaborate work on investigating this strategy.[119–121,124] Fig. 8 illustrates the formation of mesoporous thin films *via* the EISA strategy proposed by the groups of Brinker and Sanchez, respectively.

Mesoporous materials with diverse components and various morphologies have been produced. Inorganic precursors with low polymerization degrees were first dissolved in volatile solvents with weak polarity. The use of these solvents can be attributed to the loss of anisotropy for surfactants. Therefore, the cooperative assembly of surfactants and inorganic species are inhibited. It is the solvent evaporation that induces or improves the assembly at an organic–inorganic interface. Simultaneously, inorganic precursors further hydrolyze and cross-link during the solvent evaporation. High-content surfactants form liquid-crystal mesophases in the presence of inorganic oligomers at the final stage of the solvent evaporation. Organized mesostructures are generated, possibly after the formation of disordered intermediate phases. This leads to ordered mesostructures and "rigid" inorganic frameworks. Therefore, mesoporous materials are obtained after the elimination of surfactants. The final mesostructures are affected by several factors such as surfactants and their concentration, inorganic precursors, *etc*. In addition, it was found that some apparently negligible parameters, such as water concentration, processing humidity and evaporation temperatures, may show a significant influence on the final materials. The quantitative analyses of small-angle X-ray scattering in symmetric reflection (SRSAXS) and grazing incidence (GISAXS) geometries support these influencing parameters. Besides cylinder radius and lattice parameters, these techniques are claimed to provide accurate values for the polydispersity of the micelle radius, lattice parameters, and preferred orientation.[125]

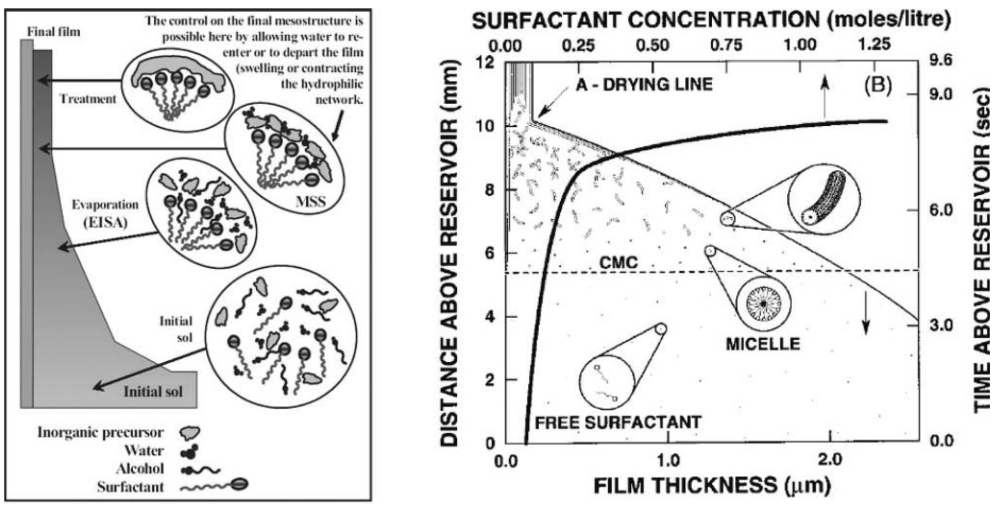

Fig. 8 Mesostructured thin-film formation by the EISA strategy proposed by the groups of Sanchez (left) and Brinker (right), respectively, reprinted with permission from ref. 17 and 120. Copyright 1997, Macmillan and copyright 2004, Wiley.

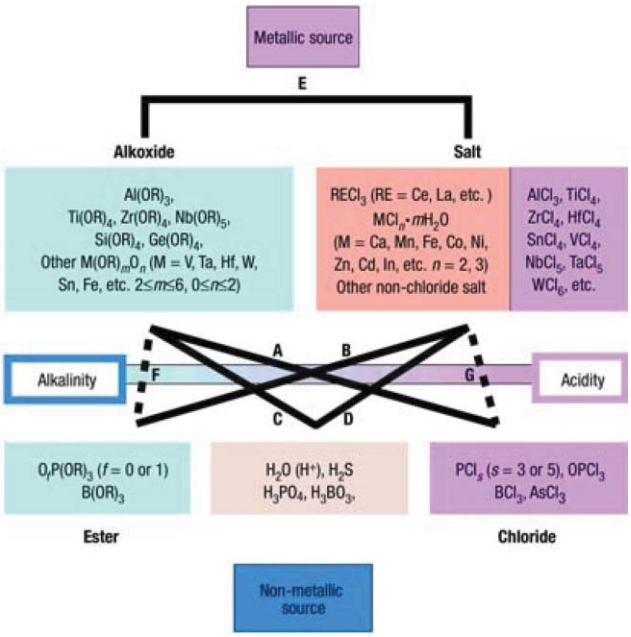

Fig. 9 General scheme of the ''acid–base pair'' concept and guided synthetic routes for mesoporous minerals, reprinted with permission from ref. 22, Copyright 2003, Macmillan.

The EISA method is a strategy that skilfully avoids the cooperatively assembling process between the precursors and surfactant templates, which facilitates surfactant-templating assembly.[30] Therefore, the interplay inside the precursors themselves which had been ignored should be paid attention to in preparing mesoporous materials, especially for non-siliceous solids.

For guiding the selection of precursors in fabricating mesoporous metal oxides with various components under non-aqueous systems, an ''acid–base pair'' concept was proposed on the basis of the compatibility of acid and base precursors.[22,126] The simple neutralization concept in the ''acid–base'' chemistry principle and the appropriate acidity self-adjusted by the precursor pairs are introduced. The ''acid–base'' synthesis route can also be used to synthesize microporous zeolites, for example, microporous aluminophosphates.[127]

First, the inorganic precursors are divided into ''acid'' and ''base'' according to their alcoholysis (here, alcohol is used as the solvent) behaviors. Inorganic metallic or nonmetallic chlorides are considered as strong ''acids'' since a large amount of acid is generated during the alcoholysis process. Hydrate metallic salts and inorganic acids (Brønsted acids) are attributed as medium acidic precursors. Metallic alkoxides and nonmetallic alkoxides (*e.g.* phosphatides) are assigned as bases because acid substances are seldom generated.

Five fundamental (A–E) acid–base pair connections between metallic sources and/or nonmetallic sources are described in Fig. 9. For convenience, nonmetallic alkoxides such as $Si(OR)_4$ and $Ge(OR)_4$ (where R is a short-chain alkyl such as CH_3, C_2H_5, C_3H_7 and C_4H_9) are listed in the metallic alkoxides column. An ''acid'' mineral precursor is designed to couple with a ''base'' counterpart, forming the ''acid–base'' pair according to their relative acidity and alkalinity on solvation. The pair not only generates a suitable acidic medium by tuning the ratio of ''acid'' to ''base'' precursors for both the inorganic–organic assembly and the gelation of inorganic precursors, but also is crucial for the homogeneous mineral composition within the whole framework. For assembling ordered mesostructures, normally the ''acid–base'' pairs formed from strong ''acid'' and strong ''base'', or strong ''acid (base)'' and medium ''base (acid)'' in non-aqueous media are required, which can be applied in the formation of homogenous multi-component inorganic precursors. Generally, the larger the acidity or alkalinity difference between the metallic and/or nonmetallic sources is, the more effectively the pairs will form and function.

In the synthesis, non-aqueous media are used to maximize the utility of this method and to promote inorganic–inorganic polymerization for assembling ordered mesostructured materials. Polar organic solvents, such as C_2H_5OH and CH_3OH, are recommended for their oxygen donating property to improve the proton transferring within the synthetic system. The various mesostructured phases can be synthesized by tuning the ratios of inorganic species to surfactants, or by using different surfactants.

Table 3 shows the examples of synthesizing various mesoporous metal phosphates through fundamental routes A–E and their derivatives. To assemble a multicomponent (I_1I_2) composite, it is necessary to match acid–base interactions of the various species presented during nucleation of the mesostructured phases in the order of the interaction $I_1I_2 \gg I_1I_1$, I_2I_2; and $O(I_1I_2) \gg OI_1$, OI_2 (here, I = inorganic species,

Table 3 Syntheses of various mesoporous metal phosphates through fundamental routes A–E and their derivatives, reprinted with permission from ref. 22

Metallic source (I_1)	Phosphorous source (I_2)	Explanation	Examples
A: $M(OR)_n$	PCl_s	$I_1I_2 \gg I_1I_1$(suppressed), I_2I_2	TiPO, ZrPO, AlPO, *etc.*
B: $MCl_n(mH_2O)$	$O_fP(OR)_3$	$I_1I_2 \gg I_1I_1$, I_2I_2	TiPO, ZrPO, NbPO, WPO, CePO, *etc.*
C: $M(OR)_n$	H_3PO_4	I_1I_2 or I_1I_1 is too strong	None
D: $MCl_n(mH_2O)$	H_3PO_4	$I_1I_2 \gg I_1I_1$, I_2I_2	AlPO, TiPO, NbPO, CePO, VPO, *etc.*
E: $MCl_n(mH_2O)$ + $M'(OR)_n$		$I_1I_2 \gg I_1I_1$, I_2I_2	VO_x, TiO_2, $Sn_xTi_{1-x}O_2$, ZrW_2O_8, *etc.*
F: $MCl_n(mH_2O)$	PCl_s	I_1I_2 is too weak	None
G: $M(OR)_n$	$O_fP(OR)_3$	$I_1I_1 \gg I_1I_2$	None
H: $M(OR)_n$ and MCl_m	H_3PO_4	$I_1I_2 \gg I_1I_1$(suppressed), I_2I_2	TiPO, AlPO, *etc.*
I: $M(OR)_n$ and MCl_m	PCl_s and $O_fP(OR)_3$	$I_1I_2 \gg I_1I_1$, I_2I_2	TiPO, ZrPO, *etc.*
J: $MCl_n(mH_2O)$	H_3PO_4 and $O_fP(OR)_3$	$I_1I_2 \gg I_1I_1$, I_2I_2	CePO, TiPO, InPO, CaPO, ZnPO, *etc.*
K: $M(OR)_n$	PCl_s and H_3PO_4	$I_1I_2 \gg I_1I_1$, I_2I_2	TiPO, *etc.*

[a] $MCl_n(mH_2O)$ means MCl_n or $MCl_n{\cdot}mH_2O$. [b] The subscripts *m*, *n*, *x*, *f* and *s* are designated as the number of the atoms.

O = organic species). For example, in the synthesis of TiPO, the starting precursors can be $TiCl_4$, $Ti(OC_3H_7)_4$ or $P(OC_2H_5)_3$, PCl_3, and the acidity can be well managed by changing the $TiCl_4/P(OC_2H_5)_3$ or $PCl_3/Ti(OC_3H_7)_4$ ratio.

This concept, together with the increased understanding on EISA strategy, sol–gel chemistry and organic–inorganic interaction, which are interdependent of each other, will pave the way for preparing ordered mesoporous nonsiliceous materials.

Recently, Watkins and co-workers reported a synthetic procedure for mesoporous silicate thin films which also separate the template formation and silicate network condensation.[128] The first step is the preparation of ordered triblock copolymer thin films doped with *p*-TSA (*p*-toluenesulfonic acid) by spin coating. This type of acid is partitioned into the hydrophilic part of the copolymer. After annealing, the template is exposed to a solution of silicon alkoxides in humidified sc CO_2 and the precursor selectively condenses *via* *p*-TSA catalysis within the acidic hydrophilic domain of the template. Mesoporosity and microporosity are generated from hydrophobic and hydrophilic parts of the triblock copolymer, respectively. This strategy may offer the possibility to prepare 2D mesoporous films with cylindrical channels oriented to the substrate surface. The resulted mesoporous silica films have excellent mechanical properties and can survive the chemical–mechanical polishing step required for device manufacturing, which is of interest to microchip designers. Moreover, the synthesis rates are fast enough for use in a microelectronics fabrication facility.

3.2 Surfactant-templating assembly with inorganic oligomers or nanoparticles

This pathway is based on the interaction occurring between surfactants and silicates to form inorganic–organic mesostructured arrangements. It is also extended to nonsiliceous mesoporous materials and even metal oxide nanotubes.

Inorganic oligomers or nanoparticles (<1 nm) can be either formed during the reaction in the synthesis system or presynthesized before assembling with surfactants. The key factors for the assembly include the control on the aggregation of inorganic precursors, and in turn, size and charge of suitable building blocks.[129] It is easy to obtain chargeable hydrated silicate oligomers provided that the hydrolysis of silicates is undertaken at a certain pH value. By contrast, the hydrolysis and condensation for most nonsiliceous inorganic species are out of control and difficult to generate 3D interlinked frameworks for stable long-range periodic mesostructures. For example, the inorganic precursors of titania have fast hydrolysis rates, and hydrolysis and condensation occur even in humid air. To obtain highly ordered mesostructures, an appropriate system is necessary to control the formation of oligomers in preparing mesoporous nonsiliceous materials. Organic chelates (acetylacetone) or organic solvents are added to inhibit the hydrolysis and obtain inorganic oligomers with appropriate sizes.[18,130] The assembly of surfactants and nanoparticles larger than 1 nm is much difficult in hydrothermal conditions, leading to disordered mesostructures in most cases.

The most popular mechanism for the formation of mesoporous solids is known as the cooperative formation mechanism which was first proposed by Stucky and co-workers.[14] It is the cooperative interaction between inorganic and organic species at molecular scale that leads to assembly to 3D ordered arrangements. Silicate polyanions can interact with cationic surfactant molecules through Coulombic forces. The polymerization of silicate species at the interface changes the charge density of inorganic layers, and in turn, the arrangement of surfactants. The matching of charge density at the surfactant/inorganic interfaces governs the assembly process. Both S^0I^0 (N^0I^0) and $S^0H^+X^-I^+$ interactions in nonionic-surfactant-templating systems are available pathways.[5,9,10]

Recently, this mechanism has been investigated by using *in situ* techniques. Goldfarb and co-workers investigated the formation mechanism of SBA-15 by using *in situ* X-band electron paramagnetic resonance (EPR) spectroscopy in combination with electron spin–echo envelope modulation (ESEEM) experiments and direct imaging and freeze-fracture replication cryo-TEM techniques.[131,132] Fig. 10(a) gives a direct-imaging cryo-TEM micrograph of SBA-15 spheroidal micelles synthesized in HCl solution at 35 °C after a short time of 5 min 13 s. After 14 min 5 s, thread-like micelles are observed (arrows in Fig. 10(b)), suggesting a continuous transformation from spheroidal micelles into thread-like micelles. Freeze-fracture replication also reveals thread-like micelles (arrows in Fig. 10(c)). Hexagonally arranged micellar bundles are then formed with dimensions which are similar to those found in the final products. The elongation of micelles is caused by the reduction of the polarity and depletion of water within micelles due to silicate adsorption and polymerization. Before high temperature hydrothermal treatment, the majority of PEO chains insert in silicate frameworks which generate micropores after the removal of triblock copolymers. Moreover, the extent of the PEO chains located within the silica micropores is dependent on the hydrothermal temperature and on the Si/P123 molar ratios.

Employing time-resolved *in situ* ^{1}H NMR and TEM, Flodstrom *et al.*[133] investigated the formation dynamics of SBA-15. Four stages were observed during the cooperative assembly: (1) silicate adsorption on globular micelles, (2) association of the globular micelles into floes, (3) precipitation of floes, and (4) micelle-micelle coalescence.

Khodakov *et al.*[134] also proposed a formation of a hydrophobic PPO core with a PEO–water–silicate corona structure in the first stage. Subsequently, cylindrical micelles pack into large domains with the solvent being replaced by condensed silicate species.

A colloidal phase separation mechanism (CPSM) for meso-/macro-topological evolution was proposed by Yu *et al.* (Fig. 11).[83] Besides the charge density matching between the surfactant headgroups and hydrolyzed inorganic oligomers, the minimization of surface free energy (F) during the coalescence and condensation of liquid crystal-like phase made up of the block copolymer/silica hybrid species should be taken into account. Although the free energy of the mesophase formation (ΔG) is responsible for the final mesostructure, the competition between ΔG and the surface free energy

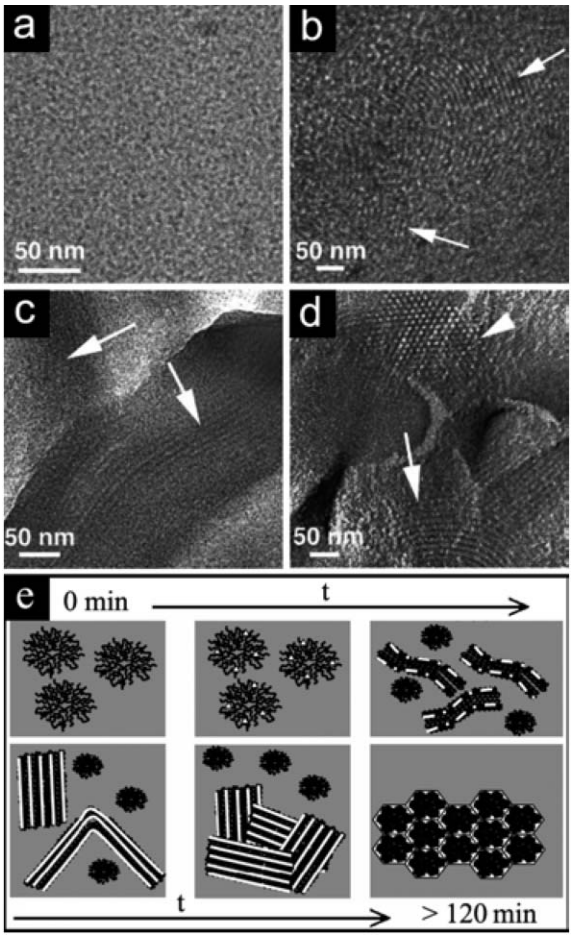

Fig. 10 Cryo-TEM images of the SBA-15 reaction in HCl at 35 °C: (a) t = 5 min 13 s, (b) t = 14 min 5 s, Freeze-fracture replication of the same system for (c) t = 16 min 27 s, (d) t = 21 min 42 s. A schematic model (e) describing the evolution of microstructures in the formation of SBA-15. The white dots/lines represent silicate oligomers. Reprinted with permission from ref. 132. Copyright 2006, American Chemical Society.

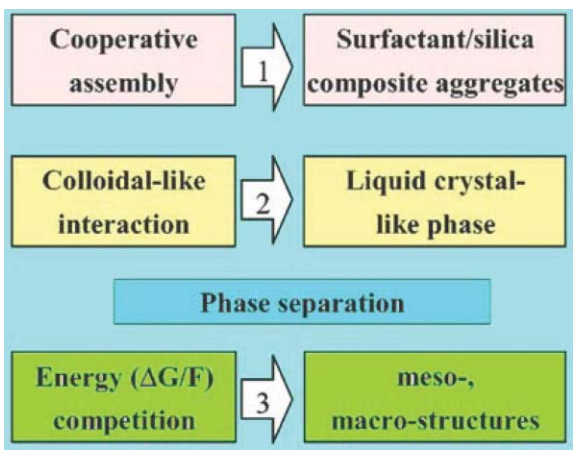

Fig. 11 Schematic diagram of colloidal phase separation mechanism, reprinted with permission from ref. 83. Copyright 2004, American Chemical Society.

(F) of this liquid crystal-like phase determines the morphologies of final mesoporous materials.

4 Design on microscale (atoms or molecules)

The synthesis includes design on the composition and crystallization. The materials with various composition display different natures and hence applications. To broaden the applications, new materials have long been developed.

4.1 Silicates and functionalization

Mesostructured silicates are easily synthesized and the mostly investigated. Compared to the other components, the clear sol–gel chemistry of silicates facilitates researchers to fully understand the formation of silicate mesostructures. Another reason lies in the fact that the research groups focusing on mesostructures have been familiar with zeolites. It is natural to apply the experiences from zeolites to stable mesoporous silicates. Diverse silicate mesoscopically periodic pore structures have been synthesized. In fact, the viewpoints here are mainly based on the knowledge of mesoporous silicates.

In general, the surfaces of pure silicate mesostructures are weakly acidic. It is found that the incorporation of metal ions into the frameworks introduced acidic and ion-exchanged functionalities and catalytic active sites.[135,136] Various metal ions, such as Al^{3+}, Ti^{4+}, V^{5+}, Ga^{3+}, Fe^{3+}, *etc.* have been incorporated into SBA-15 to enhance catalytic performances.[137–139] Different with that in zeolites which have crystal structures, the incorporation of metal ions in mesoporous silicates can not be strictly defined to intra- or extra-frameworks. A wide range of compositions with different coordination numbers and chemical environments can contribute the amorphous framework structures. For example, both tetrahedrally and octahedrally coordinated aluminium in SBA-15 are involved in the contribution of amorphous pore walls, and are ''intra-framework Al''. The former may exist inside the pore walls, while the latter may be located on the pore surface.

The frameworks of mesoporous silicates are amorphous with a large amount of hydroxyl groups on the pore surface which offer these materials great opportunities in further modification.[140] Organic-group functionalized mesoporous silicates have advantages of large surface areas, high stability, confined mesopores of inorganic solids, together with the tunable functionality of organic moieties. Two basic approaches for organic moieties incorporation have been developed, *i.e.* grafting and co-condensation methods.[6,141] Co-condensation is a synthetic approach in which silanes $(RO)_4Si$ and terminal trialkoxysilylorganosilanes $(RO)_3Si–R'$ (where R is Et or Me and R′ is a non-hydrolyzable ligand) precursors co-assemble with amphiphilic surfactants. By utilizing various methods, reactive organosilane species can be grafted on the surface or pore channels of mesoporous silicates. A wide range of functional organic groups have been incorporated to the pore walls of mesoporous silicates, including thiol, amine, epoxide, imidazole, cyanide, methyl and phenyl groups,[6,141–144] These functional sites can further react or chelate with active molecules to gain rich functionalities. Mercapto groups modified mesostructured silicates, such as

HMS, MSU and SBA-15, are very effective to adsorb Hg^{2+} ions in contaminative water and organic solvents. Stucky and co-workers synthesized SBA-15 anchored with thiol groups by co-condensation.[142] Followed by a second-step oxidation, it can be oxidized to HSO_3-SBA-15, a solid acid catalyst. This catalyst possesses a 2D hexagonal pore structure with pore size of 6 nm and specific surface area of $\sim$800 m^2 g^{-1}. The acidic capacity reaches 0.001–0.002 eq. g^{-1}, which shows great potential in catalysis.

4.2 Organosilicas

Unlike the functionalized mesoporous silicates mentioned above, where the organic ligands are anchored on the pore walls, periodic mesoporous organosilicas (PMOs) embed unique organic groups inside pore walls. They are prepared through the surfactant-templated condensation of bridged bis(trialkoxysilyl)organosilane precursors such as $(RO)_3$–Si–R″–Si–$(OR)_3$.[145,146] Both of the terminal groups in bridged bis(trialkoxysilyl) organosilanes can hydrolyze and cross-link, resulting in no cleavage of the C–Si bonds and no effect on the frameworks on account of the tetra-coordinated silicate species. Therefore organically functionalized mesoporous silicas can be produced by utilizing 100% $(R'O)_3$Si–R–Si$(OR')_3$ as silicate sources.

Owing to the similar synthetic strategy to that of mesoporous silicates, PMOs have been fabricated using nonionic surfactants as SDAs by hydrothermal and EISA methods. Enlarging pores and molding solid shapes including thin films, monoliths, spheres, polyhedra, *etc*. also proceed.[145–147] On the other hand, both chain and ring organic compounds have been integrated into inorganic matrices, including methylene, ethane, ethylene, benzene, ethylbenzene, 4-phenyl ether, 4-phenyl sulfide, *etc*.[145–149] However, the reported mesostructures (*p6m*, *Ia*$\bar{3}$*d*, *Im*$\bar{3}$*m*, *Pm*$\bar{3}$*n*, intergrowth of 3D hexagonal with cubic mesophases) are limited even with the addition of cationic surfactants, compared to their pure silica conterparts.

PMOs in the early stage were limited to short aliphatic chains (*e.g.* ethane and ethylene) or rigid and symmetrical aryl bridging groups (*e.g,* phenyl). The possible reasons lie in the chemical characteristics and physical geometrical stress.[91,150,151] The inherent hydrophobic character in the high organic-content precursors leads to either a phase separation or poor conformation, and hence, results in disordered materials. In addition, steric constraints imposed by the organic bridges may prevent efficient organization of mesostructures. For the long chain bridged organic groups or large oligomeric building units, they easily form layered mesostructures rather than stable PMOs mainly due to the intramolecular cross-linkages. Alkyl chains are claimed not longer than six carbons. The ability to maintain the mesostructured frameworks is a concern with flexible organic bridges. It is necessary to employ templates with sufficient diameters to allow uniform encapsulation by the polymerizing bridge-bonded silsesquioxanes. Well-ordered hexagonal PMOs were prepared by polymerizing phenylene-bridged silsesquioxane precursors, showing characteristics of ''rigid'' aromatic bridges and ''flexible'' methylene bridges using nonionic oligomeric surfactant templates.[151] Another approach is adding some proportion of TEOS into the organosilanes, which can be assigned to a co-condensation process of $(RO)_3$–Si–R″–Si–$(OR)_3$ and $(RO)_3$–Si–R′.[137] Successful synthesis of PMOs consisting of large heterocyclic bridging groups is a good demonstration of this.[152]

Ozin and co-workers have achieved many pioneering works on PMOs.[91,153] Organosilanes containing less hydrolyzable groups, such as $\{[(EtO)_2SiCH_2]_2[(EtO)_2SiCH]\}_2$-$\{(CH_2)_3\}$ (Fig. 12 (**1**)) can be applied to fabricating PMOs.[91] A potentiality for this kind of PMOs with pore diameter of 2.2 nm is being extended to large-pore materials templated by triblock copolymers, though they were originally synthesized by using cationic surfactants as SDAs. This is a case for an extremely high loading of organic groups. The properties of the materials can, therefore, be improved, such as low dielectric constant, high stability, hydrophobic, *etc*, which pave the way for microelectronic devices. Periodic mesoporous dendrimers (PMDs) have also been synthesized.[153] Various dendrimer building blocks (Fig. 12 (**2**) and (**3**)) with hydrolysable alkoxysilyl groups at the outmost shell assemble with triblock copolymers to yield PMDs.

4.3 Metals and sulfides

The ''true'' LCT mechanism makes it feasible to prepare mesostructured metals and sulfides. Stupp and co-workers first prepared mesostructured sulfides with oligomeric alkyl ethylene oxides.[154,155] Lyotropic surfactant liquid-crystal phases are generated with the addition of appropriate metal

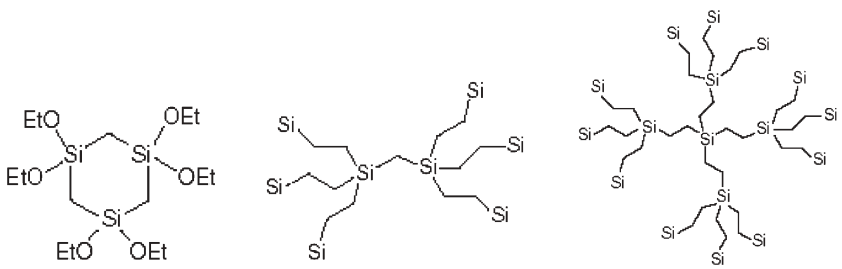

Fig. 12 The structures of partial organosilicane precursors which were reported by Ozin and co-workers in the synthesis of PMOs and PMDs, reprinted with permission from ref. 91, 146 and 153. Copyright 2003 and 2004, American Association for the Advancement of Science and copyright 2006, American Scientific Publishers.

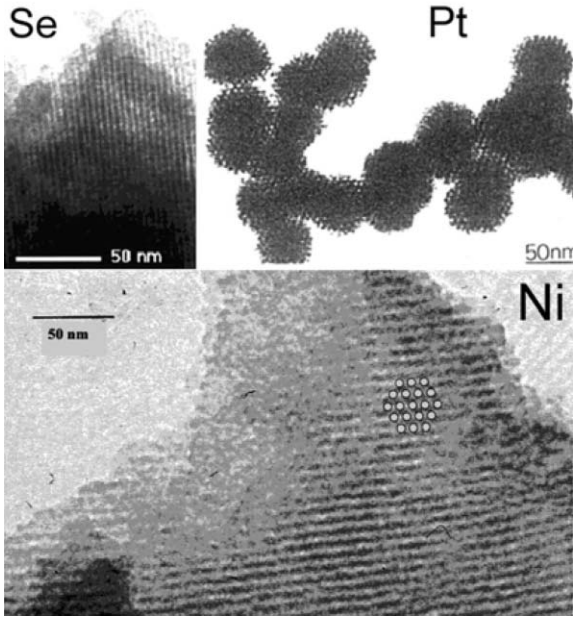

Fig. 13 Mesostructured Se, Pt and Ni from ''true'' LCT pathway, reproduced with permission from ref. 15, 156 and 157. Copyright 2001 and 2002, American Chemical Society and copyright 1997, Wiley–VCH.

ions, *e.g.* Cd^{2+}. Hydrogen sulfide or hydrogen selenide gas is then fed into the solutions to solidify the mesostructured organic–inorganic composites. A family of mesostructured solids, such as CdS, ZnS and CdSe, have been successfully synthesized. However, this process has the problem in removing surfactants. In addition, it fails in preparing other components such as Ag_2S, CuS, HgS and PbS possibly due to the unmatched interactions between metal ions or corresponding sulfide nanoparticles and surfactants. This phenomenon implies that choosing appropriate inorganic precursors is important.

Attard and co-workers created several routes to prepare mesostructured metals, metal alloys and nonmetals.[15,156–158] The metal precursors are first added to surfactant liquid-crystal phases. Ordered metal mesostructures can be fabricated either by reduction using hydrazine and a hydroboron or by electrodeposition. TEM images (Fig. 13) show that these porous metals have ordered mesostructures. In some cases, for example Pt, ordered porous nanosphere metal particles can be observed. Notably, surfactants can be removed by solvent extraction. Mesoporous metals with opened pores possess high surface areas of 20–86 $m^2\ g^{-1}$,[15,156–158] depending on the mass density, wall thickness, pore sizes, *etc*.

4.4 Nonsiliceous oxides

Although a series of ordered nonsiliceous mesostructured solids (*e.g.*, zirconium phosphates, tungstates and molybdates) have been prepared in aqueous solution, the important breakthrough did not occur until the EISA strategy was introduced to synthesize mesoporous metal oxides.[18]

Yang *et al.*[18] utilized anhydrous inorganic salts instead of alkoxides or organic metal complexes as soluble and hydrolysable inorganic precursors to construct the metal oxide mesoporous frameworks. This simple and versatile method has generated several large pore mesoporous nanocomposites, including TiO_2, ZrO_2, Nb_2O_5, Ta_2O_5, Al_2O_3, SiO_2, SnO_2, WO_3, HfO_2, and mixed oxides $SiAlO_y$, Al_2TiO_y, $ZrTiO_y$, $SiTiO_y$ and $ZrWO_y$. Those materials are relatively thermally stable probably due to their thick inorganic walls. The most important feature is the semi-crystalline frameworks where nano-crystallites nucleate within the amorphous inorganic matrices. The preparation is *via* an acid-catalyzed non-aqueous sol–gel process. The alcoholysis of inorganic salts generates $M(OEt)_nCl_m$ species with a low polymerization rate which slowly react with water in air *via* hydrolysis and cross-linkage to form mesostructures.

Guided by the ''acid–base pair'' concept, a wide variety of well ordered, large pore, homogeneous, multi-component, mesostructured solids have been synthesized, including metal phosphates, silica-aluminophosphates, metal borates, as well as various metal oxides and mixed metal oxides.[22] For example, a mixture of titanium alkoxide (ethoxide, isopropoxide or *n*-butoxide) and $TiCl_4$ were used as the precursors to prepare mesoporous titania.[126] Titanium alkoxide is used as the main titanium source and titanium chloride serves as the pH ''adjustor'' and hydrolysis–condensation ''controller''. Compared with the synthesis from a single titanium source, namely $TiCl_4$, the acidity of precursor solution is significantly and controllably reduced by the addition of titanium alkoxide which decreases the amount of $TiCl_4$ and neutralizes the acid. The added metal alkoxide is also an extra oxygen donor. Therefore, the cross-linkage and gelation of inorganic precursor molecules may be easier and better. The presence of titanium alkoxide shortens the synthesis time, improves the thermal stability and hence, maintains the mesostructure and facilitates the crystallization. Using phosphorus trichloride and zirconium propoxide as inorganic precursors, and triblock copolymers as templates, mesoporous zirconium phosphates were prepared with surface areas between 78 and 177 $m^2\ g^{-1}$ and controllable pore sizes between 2 and 4 nm.[159] Most of these mesoporous products possess semi-crystalline pore walls and relatively high thermal stability. These materials show high surface areas, uniform pore sizes and tunable periodic structures, which may lead to fascinating chemical and physical properties. Some composites such as TiPO and AlPO are stable up to 800 °C. Moreover, such materials can be easily processed as thin films, monoliths and multi-scale ordered coatings.[22]

Interestingly, when the synthesis is begun with $Ti(OC_3H_7)_3$ and $PO(C_2H_5)_3$ as precursors and triblock copolymer P123 as a SDA and followed by the controlled *in situ* crystallization of nanocomposites, the product possesses not only ordered 2D hexagonal mesostructure, but also crystalline metal oxides located within the amorphous matrix, as evidenced by XRD patterns (Fig. 14(a) and (b)).[21] The target structure of a designed mesoporous nanocomposite is shown in Fig. 14(c). The nanocomposites are made up of a large number of functional nanocrystals and a small quantity of the multi-component glass phases. It is the glass phase that helps in forming and maintaining the network, controls *in situ* crystallization of materials on a nanometer scale and ''glues'' the nanocrystals together. The mesostructures can then be retained even after the crystallization.

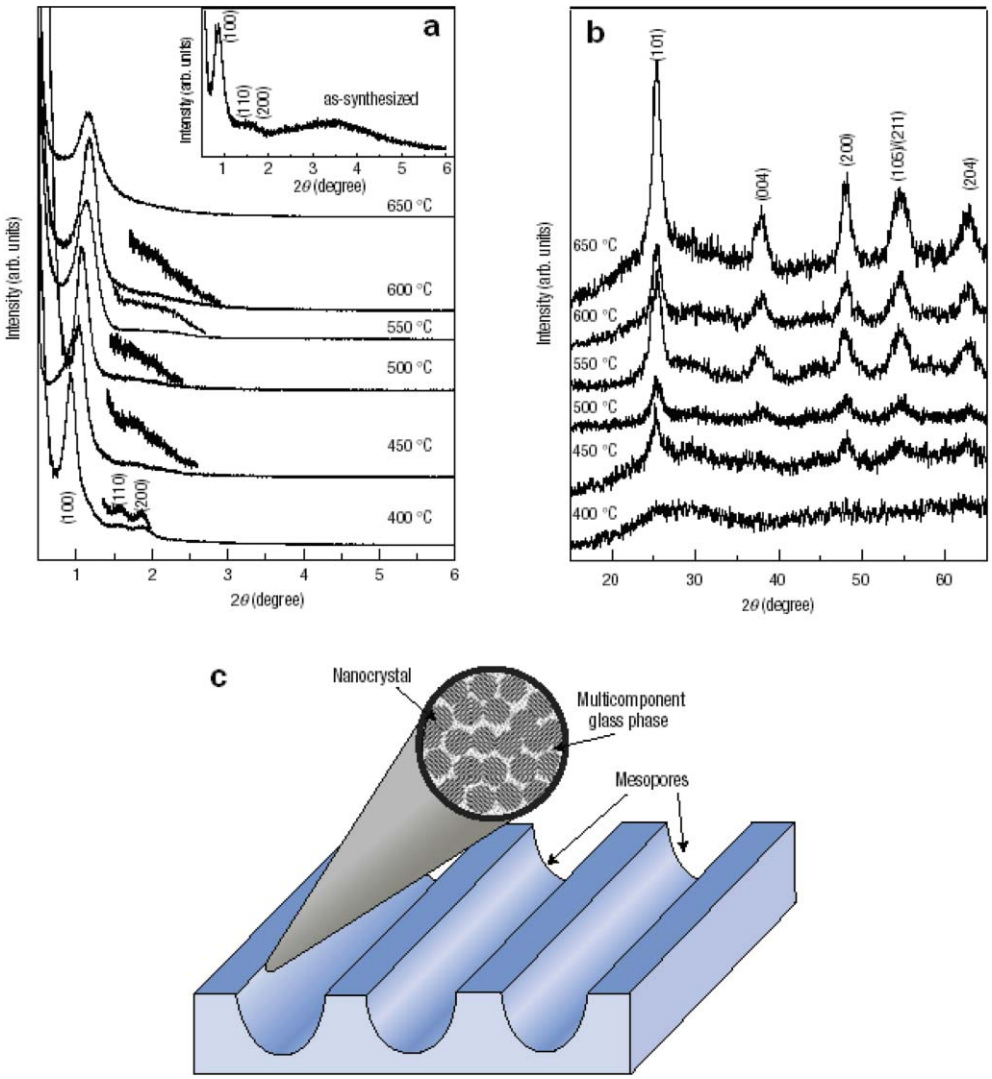

Fig. 14 (a) Powder small-angle XRD and (b) wide-angle XRD patterns of $75TiO_2$–$25P_2O_5$ materials (in molar ratio of 75 : 25) after heat treatment at 400, 450, 500, 550 and 650 °C. The inset of (a) is small-angle XRD pattern of the as-synthesized material. (c) Target structure of designed mesoporous nanocomposites. Reprinted with permission from ref. 21. Copyright 2004, Macmillan.

4.5 Phosphates

Phosphates ($AlPO_4$-*n*, SAPO-*n*, *etc.*) attract enormous attention due to impressive performances in heterogeneous catalysis.[7,29] However, the small micropores (<2 nm) limit their applications towards macromolecules. A supramolecular-templating approach is much expected to synthesize mesoporous phosphates. Most mesoporous phosphates, especially thermally stable phosphates (*e.g.* zirconium organophosphate), are templated by cationic surfactants.[160–162] Lamellar or microporous phosphates are produced by using neutral long-chain alkyl amines as SDAs.[163] Tiemann and Froba[164] prepared mesoporous aluminophosphates with pore sizes smaller than 4 nm in the presence of long-chain alkyl amines under basic non-aqueous conditions. The stability is improved by post-treatment in water vapor.

Tian *et al.*[22] first reported large-pore (~10 nm) mesoporous phosphates by using triblock copolymers as SDAs *via* the EISA strategy. $AlCl_3$ and H_3PO_4 serve as inorganic precursors due to the formation of effective "acid" and "base" pairs. By contrast, only disordered mesoporous aluminophosphates are obtained when other precursors are selected, for example, $AlCl_3/OP(OCH_3)_3$ and $Al(OC_4H_9)_3/PCl_3$. On the basis of the "acid–base pair" route, aluminium organophosphonates (AOPs) have been synthesized by using $(HO)_2OPCH_2PO(OH)_2$ and $AlCl_3$ with an initial molar Al : 2P ratio of 1 : 0.75 in the presence of oligomeric surfactants and triblock copolymers. 2D Hexagonal ordered mesoporous AOPs can be obtained.[165] These mesoporous AOPs are similar to PMOs from the viewpoint of organic–inorganic hybrid structures. The C–P bonds can be retained after extracting the surfactants. The resultant materials have uniform mesopores (3.3–9.2 nm) and high BET surface areas (up to 500 $m^2\ g^{-1}$).

4.6 Polymers and carbons

The preparation of mesoporous carbon materials with ordered open pore structures from a supramolecular-templating approach is extremely difficult in solution and remains challenging owing to the intrinsic characteristics of organic

molecules and the high formation energy of C–C bonds. Most of the researches were focused on mesoporous carbon replicas prepared by a mesoporous silica hard-templating method, *via* carbonization of sucrose-filled ordered mesoporous silicates, and then removal of the silica frameworks by HF or NaOH.[166] The replicas obtained from the time-consuming and costly procedure are constructed as ordered nanowire, nanorod or nanotube arrays, replicating the ordered structures of mesoporous silicates. Therefore, a soft surfactant self-assembling approach towards ordered mesoporous carbons with zeolite-like frameworks is desirable.

Hillmyer and co-workers used low-molecular-weight thermosetting epoxy as an organic precursor and diblock copolymer poly(ethylene oxide)-*block*-poly(ethylethylene) (PEO-*b*-PET) as an amphiphilic template to synthesize ordered polymer nanostructures.[167] However, no porosity was reported. Disordered mesoporous polyacryonitrile structure can be obtained from self-assembly of the reversed triblock copolymer $PO_{19}EO_{33}PO_{19}$.[168]

More recently, Dai and co-workers[169] successfully prepared ordered mesoporous carbon films with open framework structures by using resorcinol and formaldehyde as carbon sources and diblock copolymer poly(styrene)-*block*-poly(4-vinylpyridine) (PS-*b*-P4VP) as a template. Similar results were reported by Tanaka *et al.*,[170] in which the same carbon precursor and Pluronic F127 were used for organic–organic self-assembly. Triethyl orthoacetate was added as a carbon co-precursor, which may decrease the polymerization rate of resorcinol and formaldehyde under strong acid conditions and enhance the interaction between them and surfactant templates.

Consequently, the interactions between both organic precursors and templates, and the organic precursors themselves should be considered in the organic–organic assembly for preparing ordered mesoporous polymers and carbons with diversified structures. We independently demonstrated a reproducible synthesis of highly ordered mesoporous polymers and carbons from an organic–organic EISA process of low-molecular-weight and water-soluble phenolic resins (resols) and commercial triblock copolymers PEO-PPO-PEO.[171] The schematic presentation of the synthesis is shown in Fig. 15. From the viewpoint of synthesis, these mesoporous polymers and carbons are excellent examples to expatiate the EISA process.

The initial homogeneous solution is prepared by dissolving the triblock copolymers and resol precursors in ethanol. Resol precursors have 3D network structures and plenty of hydroxyl groups (–OH), which are polymerized by phenol and formaldehyde under alkaline conditions. They can strongly interact with the PEO blocks of triblock copolymer templates *via* hydrogen bonds. The assembly of phenolic resins and copolymer templates occurs readily to form ordered mesostructures without macrophase separation. The preferential evaporation of ethanol progressively enriches the concentration of copolymers and drives the organization of resol–copolymer composites into an ordered liquid-crystal mesophase. Furthermore, the ordered mesophase is solidified by the cross-linkage of resols, which can be easily induced by thermopolymerization. It should be noted that the cross-linking and polymerizing processes of the phenolic resin frameworks are separated from the assembly with surfactants. This is an important feature of EISA strategy. It is quite different from a cooperative formation assembly mechanism, where the surfactant-templating assembly and polymerization of inorganic oligomers occur cooperatively and simultaneously.

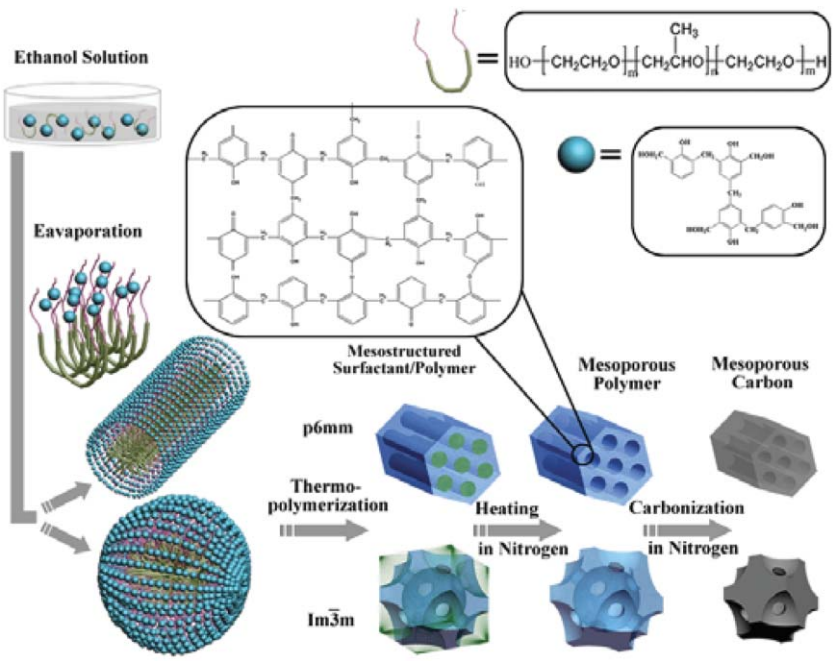

Fig. 15 Schematic diagram of the synthetic procedure for mesoporous polymer and homologous carbon frameworks, reprinted with permission from ref. 171. Copyright 1997, Wiley–VCH.

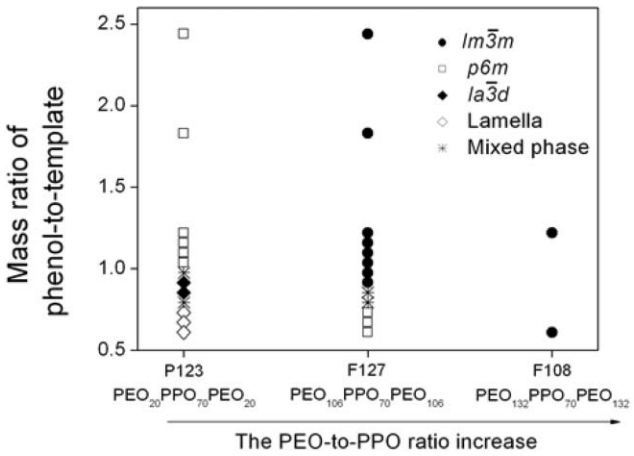

Fig. 16 Phase diagram for as-made mesostructured polymer and carbon materials. Reprinted with permission from ref. 172. Copyright 2006, American Chemical Society.

The triblock copolymer templates can thermally decompose and yield large mesoporosity of polymer resins by calcination under an inert atmosphere. In addition, the polymer resin frameworks are stable enough to resist the deformation caused by the removal of templates. Further increasing the heating temperature leads to a framework transformation to carbons with ordered homologous mesostructures.

A family of highly ordered mesoporous polymer resins and carbons have been synthesized, including mesostructures with lamellar, 2D hexagonal *p6m* (FDU-15), body-centered cubic *Im*$\bar{3}$*m* (FDU-16) and bicontinuous cubic *Ia*$\bar{3}$*d* (FDU-14) symmetries, which are obtained by simply varying the phenol/triblock copolymer ratios and PEO/PPO ratios in the templates (Fig. 16).[172] Fig. 17 shows the SAXS patterns and TEM images of well-ordered FDU-16 with 3D cubic *Im*$\bar{3}$*m* symmetry. The resols may be favored to interact with hydrophilic PEO blocks in the copolymers, which causes changes of hydrophilic/hydrophobic ratios in the resol–surfactant mesophases, and hence a difference in the interfacial curvatures. Higher ratios favor the formation of mesostructures with higher curvatures. The mesoporous polymer resins exhibit highly ordered structures, high surface areas ($\sim$670 m^2 g^{-1}), large pore volumes ($\sim$0.65 cm^3 g^{-1}) and uniform, large pore sizes ($\sim$7.0 nm). Further heating to a temperature above 600 °C transforms the mesoporous polymers to the homologous carbon frameworks. Ordered mesoporous carbon products show high surface areas ($\sim$1500 m^2 g^{-1}), large pore volumes ($\sim$0.85 cm^3 g^{-1}) and uniform, large pore sizes ($\sim$4.9 nm), as well as very thick pore walls (6–8 nm). In addition, the open carbon frameworks with covalently bonded construction and thick pore walls exhibit high thermal stability (>1400 °C). Compared with conventional mesoporous silicates, the new families of ordered mesoporous organic polymers and inorganic carbon solids offer great opportunities with applications emerging in adsorption, catalysis, drug delivery, electrodes, and bioengineering.

The organic mesoporous materials and homologous carbons with open frameworks can also be prepared in aqueous media.[173] The preformed resols first cooperatively assemble with triblock copolymers, leading to block-copolymer–resin mesophases in dilute solution at pH *ca.* 9.0. Further polymerization and carbonization direct the mesoporous polymer and homologous carbon molecular sieves to desired mesostructures (hexagonal *p6m*, cubic *Im*$\bar{3}$*d* symmetries).

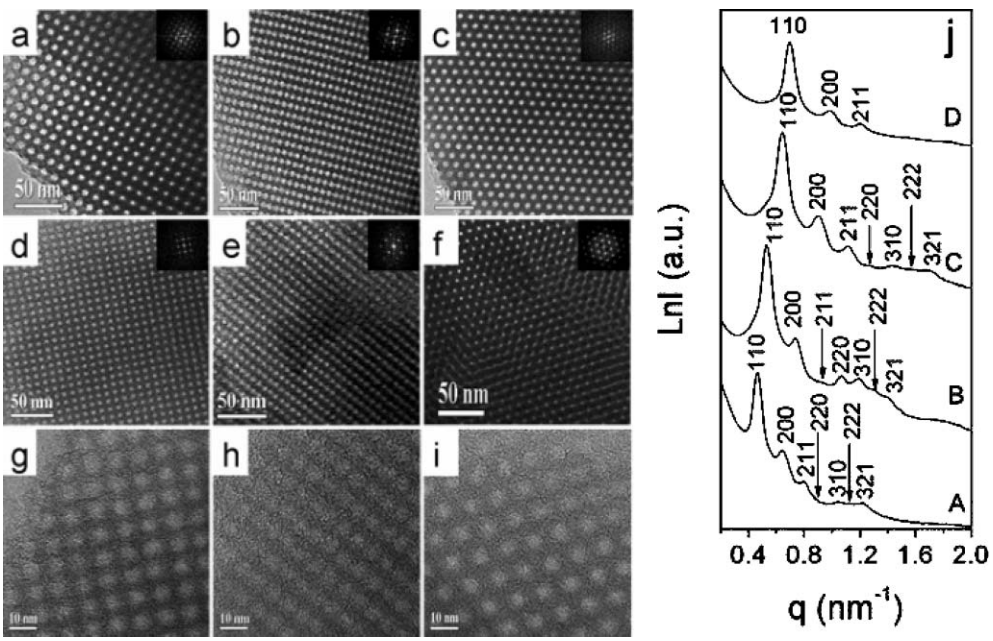

Fig. 17 TEM images (a)–(f) and high resolution transmission electron microscope (HRTEM) images (g)–(i) of mesoporous materials FDU-16 prepared by using F127 as a template *via* the EISA method after calcination at 350 °C under 2.4% O_2–N_2 (a, b, c) and at 1200 °C under Ar (d, e, f, g, h, i), viewed along [100] (a, d, g), [110] (b, e, h) and [111] (c, f, i) directions. The insets are the corresponding fast Fourier transform (FFT) diffractograms. SAXS patterns (j) of mesoporous materials FDU-16: as-made FDU-16 (A), calcined at 350 °C under 2.4% O_2–N_2 (B), at 600 °C under Ar (C) and at 1200 °C under Ar (D). Reprinted with permission from ref. 172. Copyright 2006, American Chemical Society.

Different from the EISA method, the aqueous pathway can involve hydrocarbons such as hexadecane and decane as swelling agents to enlarge the pore sizes of highly ordered mesoporous polymers and carbons. Moreover, the morphologies and particle sizes can be controlled by PEO/PPO ratios and concentration of triblock copolymers. The resulting mesoporous carbon materials can possess a pellet-like morphology in the size of 1–5 mm and a rod-like particle morphology in the size of 5–200 μm. These phenomena are reminiscent to those in the hydrothermal synthesis of mesoporous silicates.

The similarity of the organic–organic self-assembly to the inorganic–organic route makes it possible to extend the compositions and structures of mesoporous polymers and/or carbons. It is the organic precursor that dominates the whole process.

It is worthy of note that this organic–organic assembling pathway is general and can be extended to prepare hybrid mesoporous materials. Very recently, highly ordered mesoporous polymer–silica and carbon–silica nanocomposites with interpenetrating networks have been successfully synthesized by using resol polymer as an organic precursor, prehydrolyzed TEOS as an inorganic precursor and triblock copolymer F127 as a template.[174] A triconstituent co-assembly process has been proposed and the detailed characterizations show that ordered mesoporous nanocomposites have ''reinforced concrete''-structured frameworks. The composition diagram of both carbon and silica can be drawn in a range from 0 to 100%. The presence of inorganic silicates in the nanocomposites dramatically inhibits framework shrinkage during calcination, resulting in highly ordered large-pore mesoporous carbon–silica nanocomposites. Combustion in air or etching in HF solution can remove carbon or silica in the carbon–silica nanocomposites, and yield ordered mesoporous pure silica or carbon frameworks, respectively. Ordered mesoporous carbons can then be obtained with large pore sizes of $\sim$6.7 nm, pore volumes of $\sim$2.0 $cm^3\ g^{-1}$ and high surface areas of $\sim$2470 $m^2\ g^{-1}$.

4.7 Crystallization

For many applications, such as photocatalysis, the percentage of nanocrystallites makes a significant difference. One has to address this problem probably by either choosing suitable inorganic precursors or employing a different thermal treatment process.

As mentioned above, Zhou and co-workers demonstrated a synthetic methodology of a surfactant-templating approach followed by the controlled *in situ* crystallization to create ordered mesoporous composites with crystalline oxides/amorphous phosphates frameworks.[21] Ordered mesoporous ceramics with fully crystallized ZrO_2 and TiO_2 have been fabricated.

Mesoporous TiO_2 optical thin films with fully nanocrystalline anatase frameworks which are ideal hosts for energy transfer applications, have been fabricated by employing a so-called two-step ''delayed rapid crystallization'' thermal treatment.[175] A rapid but homogeneous crystallization at low temperature is conducted to stabilize matrices and form anatase frameworks. These TiO_2 thin films can retain most of their meso-skeletons up to 700 °C and emphasizes the advantage of this procedure on stabilizing transition metal oxide mesoporous materials, over extended crystallization at high temperatures.

Katou *et al.*[176] have prepared highly crystalline niobium–tantalum mixed oxide mesoporous solids which are supported by embedded carbon rods. These mesoporous solids exhibit single crystal features. This method may be applied to crystallization of other mesoporous oxides, but their crystallization temperature may be limited to a particular range (550–750 °C).

5 Design of mesostructures

Mesoporous materials can be divided into ordered and disordered structures from the viewpoint of pore/channel packing regularity.

5.1 Ordered 2D mesostructures

Highly ordered mesoporous materials SBA-15 (*p6m*) can be synthesized by using nonionic surfactants such as alkyl PEO oligomeric surfactants, star diblock copolymers and triblock copolymers as templates under acidic conditions.[36] Triblock copolymers are effective surfactants with the most optimal being Pluronic P123. Other block copolymers can also serve as templates such as P104 ($EO_{27}PO_{61}EO_{27}$), P85, P65, L64 ($EO_{13}PO_{30}EO_{13}$) and B50-1500, but the synthesis temperature is higher. Hydrothermal treatment (100 °C for 3 days) is required when nonionic oligomeric surfactants serve as templates. The synthesis of SBA-15 normally requires 24 h, longer than that of MCM-41.

N_2 Sorption isotherms show that SBA-15 materials have well-uniform pore size distributions and perfect cylinder channel pores. The pore wall thickness can be controlled from 3.1 to 7 nm, much larger than that of MCM-41. This may be one of the reasons for higher thermal stability and hydrothermal stability of SBA-15 than MCM-41. The SBA-15 mesostructures can be thermally stable up to 1000 °C. Calcined SBA-15 retains most of its structure after being heated in boiling water for more than one week. Mesoporous silicas SBA-15 with small pore sizes can be templated by alkyl PEO surfactants, *e.g.* $C_{16}EO_{10}$, under acidic conditions.

It has been revealed that the wall structure of SBA-15 is quite different from that of MCM-41, although the two materials have the same space group (*p6m*). A large number of intraframework micropores, and even small mesopores are distributed inside the pore walls of SBA-15. No diffraction peaks assigned to these micropores are detected in the XRD patterns due to their disordered arrangements. Nitrogen sorption techniques reveal these small pores with sizes between 1 and 3 nm.[177] The intraframework pores are also verified by nanocasting metal oxide, metal sulfide, carbon and even metal negative replicas inside SBA-15 mesochannels.[166,178] The final nanowire or nanorod arrangements are connected and supported by nanorod pillars. In contrast, only separated nanowires are replicated by MCM-41 hard templates.[179]

Direct images of disordered arranged micropores are difficult to obtain by HRTEM. A possible method is filling heavy metals inside the pore channels so that reversed

mesopores can be imaged by HRTEM owing to high contrast. Alternatively, relatively large mesopores inside pore walls can be directly observed.[180] Therefore, understanding on the origin of micropores and small mesopores inside pore walls is important.

It is believed that triblock copolymers not only play a role of templates but also insert into the silica framework with PEO blocks and form organic–inorganic hybrid frameworks.[25,181] After the removal of triblock copolymers upon calcination, micropores and small mesopores are left in the frameworks and tunnels are generated between primary mesopores. This character can be used to expand the mesoporous material family with attractive pore structures.

During hydrothermal treatment at high temperature, PEO segments become hydrophobic and draw back from the silica walls. The enlarged surfactant micelles result in large-pore SBA-15 and low micropore volumes. However, small mesopores inside pore walls are generated from the distortion of micelles during the heating procedure rather than the simple insertion of PEO chains inside inorganic pore walls.[180] In contrast to shrunken micropores, small mesopores inside pore walls become large at high temperature. Fan *et al.*[180] developed an approach by introducing TMB into embryo mesostructured SBA-15 to form 3D SBA-15 with the average mesostructure of hexagonal *p6m*. The swollen micelles of triblock copolymers and TMB expand the micropore zone inside the inorganic pore walls. After high-temperature hydrothermal treatment, the micropore region in the complementary pores almost disappears, leaving only relatively large (2–8 nm) connections or mesotunnels with random distribution as evidenced by TEM images (Fig. 18). Hydrothermally treating SBA-15 at 80 °C, Galarneau *et al.*[117] also observed the elimination of microporosity and the existence of secondary mesoporosity of SBA-15. On the other hand, the isolated spheres packing model of large-molecular-weight block copolymers may result in no micropore connections between mesopores and hence no mesoporosity, as mentioned above. The insertion of long PEO chains inside silica pore walls may help these block copolymers to form tunnels connecting primary mesopores of silicates. Ordered mesoporous silica with opened pores and large sizes (>30 nm) are desirable.

The complementary porosity, including both micropores and smaller mesopores, of SBA-15 can be controlled by hydrothermal temperature and time during the synthesis and calcination process.[182] Prolonging the time can enhance the mesoporosity of the silica walls and thus enable more connections of the main channels. Such connections can be retained to a significant extent after calcination at 800 °C, but are possibly completely eliminated at 1000 °C. Kaliaguine and co-workers studied the diffusion of small probe molecules such as *n*-heptane through the pore structure of intrawalls.[182,183] The diffusivity and activation energy depend significantly on the relative contents of micropores and secondary mesopores. If the micropore content is high, the diffusion is low, suggesting a micropore-diffusion-controlled process. It will change to the secondary-mesopore-controlled one as this kind of complementary pores is dominant in the intrawall structures. The diffusivity of the mesopores exhibits a 3–4 times larger value than the micropores.

Mesoporous silica SBA-15 calcined at 900 °C can retain an ordered mesostructure after water steam treatment at 600 °C for 24 h or at 800 °C for 6 h[184] related to the improved cross-linking degrees of surface silanol groups and the elimination of micropores. These small pores can also be blocked by surface modification with octyldimethylsilyl.[181] This brings about a more obvious decrease in BET surface area than that in MCM-41 that has no micropores in the framework.

Su and co-workers have obtained a well-ordered mesoporous silica CMI-1 from $C_{16}EO_{10}$ in a relatively wide range of surfactant concentrations under mild acidic conditions.[50]

5.2 Ordered 3D mesostructures

Mesoporous silica FDU-5 has the same structure as MCM-48, which is defined by a so-called minimum surface, gyroid (G-surface). The minimum surface divides the space into identical but separated two-group 3D pore channels, forming a cubic bicontinuous $Ia\bar{3}d$ mesostructure. FDU-5 mesoporous silica of bicontinuous cubic mesostructure is synthesized using triblock copolymer P123 as a template, nonpolar solvent such

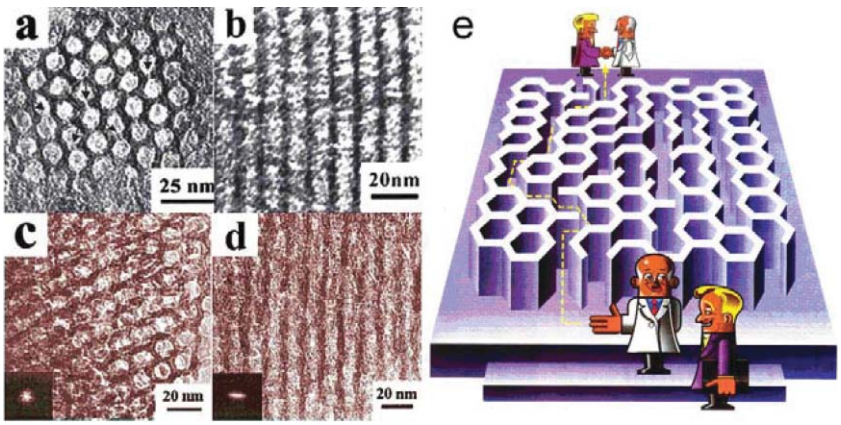

Fig. 18 HREM images and electron diffraction patterns of calcined 3D mesoporous SBA-15 prepared at 130 °C (a, b) without TMB and (c, d) with TMB viewed along the (a, c) [001] and (b, d) [110] directions, reprinted with permission from ref. 180. Copyright 2001, American Chemical Society. Cartoon scheme (e) for 3D SBA-15 with large mesotunnels.

as benzene, toluene or ethylbenzene or organosilane such as MPTMS as an additive, *via* the EISA strategy with/without solvothermal post-synthesis under acidic conditions.[55,61] The reciprocity between organic agents and surfactants can increase the hydrophobic/hydrophilic ratio and hence result in the phase transformation from *p6m* to $Ia\bar{3}d$. The FDU-5 mesostructure has a large uniform pore size of about 8.1 nm and a high surface area of 804 $m^2\ g^{-1}$. Ryoo and co-workers[57] reported the synthesis of KIT-6 mesoporous silica with $Ia\bar{3}d$ mesostructure by using triblock copolymer P123 as a template and *n*-butanol as an additive *via* a hydrothermal method. Other triblock copolymers which can template 2D hexagonal mesostructures can also be used as SDAs to prepare $Ia\bar{3}d$ mesostructures. These large-pore mesoporous silica materials have been utilized as good hosts to cast mesoporous carbons, metal oxides and metal sulfides with reversed bicontinuous cubic structure ($Ia\bar{3}d$).[57,185]

Apart from the gyroidal pore structure, sphere caged pores are detected in the other cubic mesostructures. Both pore sizes and window (entrance) sizes are important. The latter is a key factor for the applications in which mass transportation and diffusion are necessary. Generally, the pore diameter and the pore window size should be calculated from the adsorption and desorption branch of N_2 isotherms, respectively.

The body-centered cubic SBA-16 mesostructure (space group $Im\bar{3}m$) was first reported by Zhao *et al.*[36] by using triblock copolymer F127 as a template in 2 M HCl solution. A suitable and reproducible synthesis with a comparatively slow precipitation rate was recently reported in acidic aqueous synthesis media (0.5 M HCl).[112] Triblock copolymers with relatively large EO chains can serve as templates, such as F127, F108 and F98, but triblock copolymers such as F88 ($EO_{104}PO_{39}EO_{104}$) and F68 with overlong EO chains are seldom used. Assisted by inorganic salts such as KCl, NaCl, Na_2SO_4 and K_2SO_4, highly ordered SBA-16 can be easily prepared by using F127 as a template after hydrothermal treatment at 85–100 °C. Mesoporous silica IBN-1 with 3D cubic $Im\bar{3}m$ structure was templated by F127 with the aid of the fluorocarbon surfactant FC-4.[53] By comparison, the EISA method is more easy and facile to prepare SBA-16 mesostructures.[74]

TEM analysis confirms that the SBA-16 mesostructure has the body-centered cubic symmetrical packing of sphere cages.[20] The pore size is calculated to be 5.4 nm using the traditional BJH (Barrett–Joyner–Halanda) model of SBA-16 with a unit cell parameter of 16.6 nm.[36] According to non-local density functional theory (NLDFT), the sphere cage size of SBA-16 is 8.5 nm and the minimum wall thickness is 5.9 nm.[186] Thick pore walls indicate that sphere cages are interconnected by micropores or small mesopores. Otherwise surfactants which occupy the voids in as-made silica frameworks can not escape during calcination and porosity can not be obtained. Van der Voort *et al.*[187] reported the presence of micropores but no direct images from TEM analysis have been reported.

Increasing hydrothermal temperature and prolonging hydrothermal time can enlarge the entrance sizes of SBA-16.[188] Other methods that can uniformly expand pore entrances include the use of blending triblock copolymers such as P123 and F127 and H_2SO_4 post treatment.[188,189] The latter method can even lead to pseudo-cylindrical mesopores with the maintenance of the overall cubic symmetry of SBA-16.

Triblock copolymer B50-6600 ($EO_{39}BO_{47}EO_{39}$) with a more hydrophobic PBO segment can template the formation of the FDU-1 mesostructure.[69] This large caged material was originally assigned to the space group $Im\bar{3}m$ with a_0 = 22 nm, as evidenced by the well-ordered XRD patterns (Fig. 19(a)). It has sparked a great deal of researches thereafter. On the basis of HRTEM images and SAXS patterns (Fig. 19(b)), Jaroniec and co-workers suggested that FDU-1 prepared by themselves was a face-centered cubic $Fm\bar{3}m$ structure with 3D hexagonal intergrowth and the cubic phase was the main constituent.[68] However, the XRD (SAXS) patterns in these two papers are different. Pore cage sizes of FDU-1 can be adjusted in the range from 8.7 to 11.7 nm by increasing the reaction temperature from 25 to 90 °C (Fig. 19(c)).[68] By adjusting the hydrothermal temperature and time, FDU-1 materials can be afforded with tailored pore cage diameters and pore entrance sizes from about 9.5 to 14.5 nm and from below 4 to about 8 nm, respectively, in the presence of inorganic salts.[190] The uniformity of both cages and entrances of FDU-1 can be enhanced by doubling the amount of $EO_{39}BO_{47}EO_{39}$ copolymer, adding NaCl, or reducing the acidity of the synthesis gel.[191] Moreover, the FDU-1 mesostructure displays high thermal and hydrothermal stability.[192]

SBA-12 mesoporous silica was synthesized by using oligomeric alkyl PEO Brij 76 surfactant as a template.[36] The BET surface area, pore volume and mean pore size are 1150 $m^2\ g^{-1}$, 0.83 $cm^3\ g^{-1}$ and 3.1 nm, respectively. The XRD pattern could be easily mixed up with the 3D hexagonal $P6_3/mmc$ mesostructure but TEM images show the intergrowth of hexagonal close packing (hcp) with cubic close packing (ccp) mesostructures.[193] The corresponding pure ccp phase should be a face-centered cubic $Fm\bar{3}m$ mesostructure. Fortunately, large domains of the cubic phase were found in a mercapto group modified SBA-12 material by Spanish scientists. Clear electronic micrographs make it feasible for resolving its mesostructure through electron crystallography. It shows a face-centered mesostructure with a unit cell parameter of 8.2 nm. Each sphere cage is connected with twelve adjacent cages by small windows.[193]

FDU-12 presents a face-centered cubic mesostructure (space group $Fm\bar{3}m$) without intergrowth of a 3D hexagonal mesostructure.[63] Mesoporous silica FDU-12 was synthesized by using block copolymer F127 or F108 as a template and TMB together with inorganic salts such as KCl as additives. TMB molecules here, associate with PPO segments to improve the hydrophobicity, that can reduce the interaction between triblock copolymers and silicate species and seemingly favor the formation of the cubic mesostructure. Inorganic salts may stabilize mesostructure regularity. The synergistic action of TMB and KCl is important for the synthesis of FDU-12.

The cage sizes of FDU-12 can be directly measured from the thin edges of the particles and the results are in good agreement with those calculated from corresponding nitrogen adsorption isotherms, as shown in Fig. 20. The cavity sizes of FDU-12 are as large as 10–12.3 nm. Lowering the synthesis temperature can further enlarge the pore cage size from 14 to

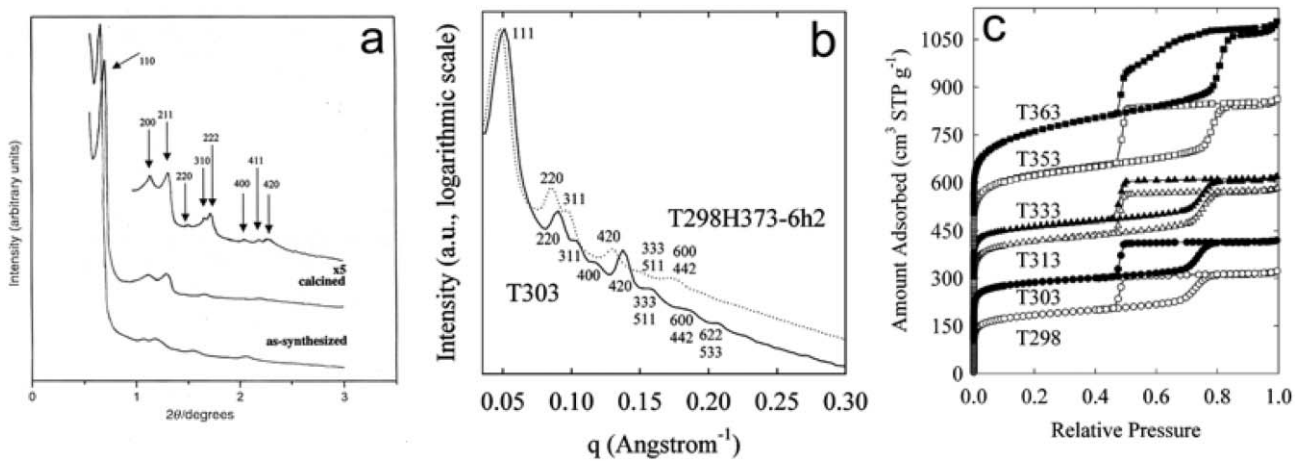

Fig. 19 (a) XRD patterns of as-synthesized FDU-1 and FDU-1 calcined at 550 °C. (b) SAXS patterns for FDU-1 silica samples synthesized at 30 °C (T303) and synthesized at 25 °C followed by hydrothermally treatment at 100 °C for 6 h (T298H373-6h2). (c) Nitrogen adsorption isotherms for FDU-1 samples synthesized at 30 °C (T303), 40 °C (T313), 60 °C (T333), 80 °C (T353) and 90 °C (T363). The isotherms for T303, T313, T333, T353 and T363 samples were offset vertically by 100, 200, 300, 400 and 500 cm^3 STP g^{-1}, respectively. Reprinted with permission from ref. 68 and 69. Copyright 2003, American Chemical Society and copyright 2000, Royal Society of Chemistry.

22 nm.[100] Besides, filling gold nanoparticles inside the pore channels reflects the true shapes of pore structures after the removal of FDU-12 hard templates. The resultant dumbbell-like gold nanoparticles are connected by gold nanorods (Fig. 20(d)). The measurement of diameters for sphere nanoparticles and nanorods gives sphere cages and window sizes of FDU-12, respectively, provided that the growth of gold nanoparticles inside the mesochannels does not distinctly destroy the pore structures. Interestingly, the size of the windows can be continuously adjusted in the range of 4–9 nm by increasing the hydrothermal treatment temperature from 100 to 140 °C.[63] It is a key factor for the immobilization of enzymes, and fabrication of cubic mesoporous carbon replicas with ordered large pores.

By using low HCl concentration in aqueous solution, cubic mesoporous silica KIT-5 with $Fm\bar{3}m$ symmetry was templated by the same triblock copolymer F127.[64] However, a remarkable discrepancy has been observed in XRD patterns of these two materials (FDU-12 and KIT-5) with the same face-centered cubic $Fm\bar{3}m$ mesostructure (Fig. 21). A strong 311 and unresolved 200 and 400 diffraction peaks are observed for FDU-12 while KIT-5 exhibits a strong 220 diffraction peak and weak 200 and 311 reflections. This phenomenon implies a difference of the pore configuration. This difference is expected

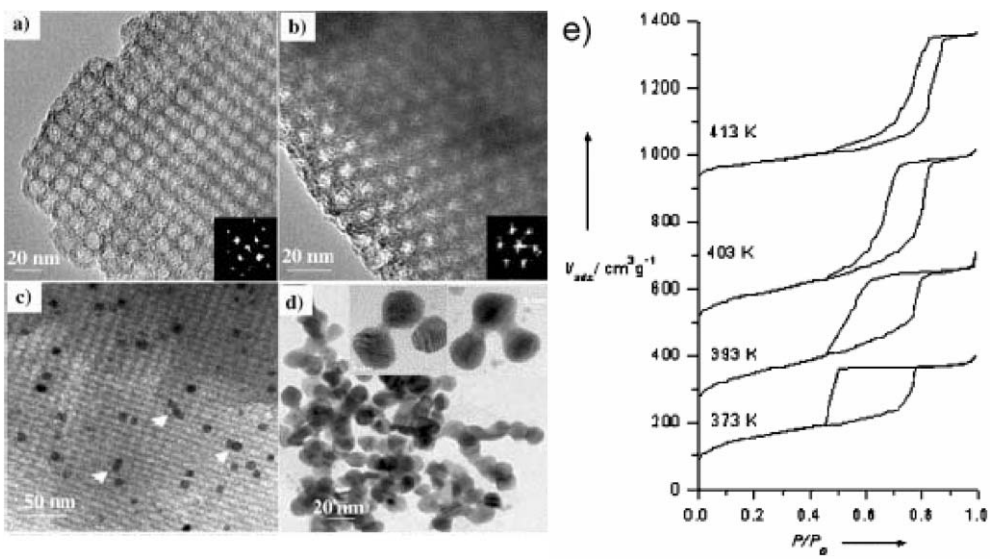

Fig. 20 TEM images (a) and (b) of FDU-12 hydrothermally treated at 100 °C recorded along the [100] and [111] directions (insets show Fourier diffractograms), respectively. TEM images (c) of Au/FDU-12 (hydrothermally treated at 100 °C) and (d) Au nanocrystals after the removal of the silica frameworks. The insets show enlarged TEM images of dumbbell-like Au nanoparticles formed inside FDU-12 hydrothermally treated at 100 °C (left) and at 130 °C (right). N_2 sorption isotherms (e) of FDU-12 samples hydrothermally treated at 100, 120, 130 and 140 °C. The adsorption isotherms for the last three samples are shifted by 200, 450, 900 cm^3 STP g^{-1}, respectively. Reprinted with permission from ref. 63. Copyright 2003, Wiley–VCH.

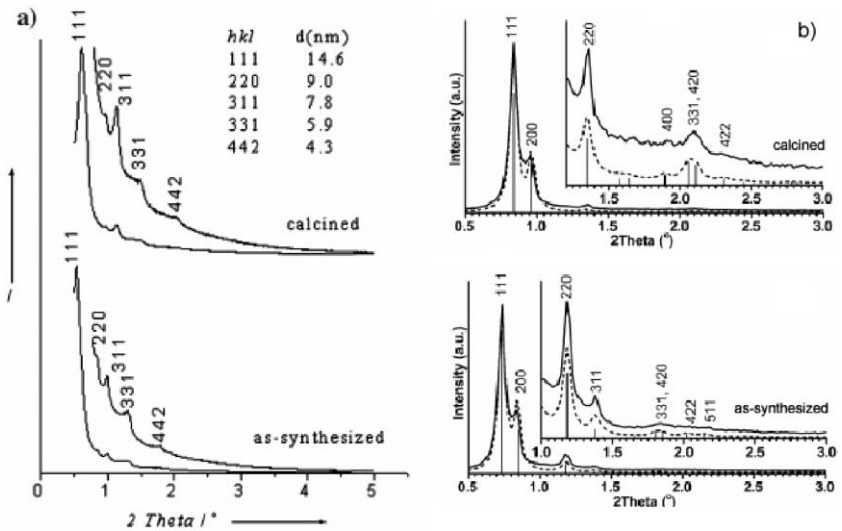

Fig. 21 (a) XRD patterns of as-synthesized and calcined FDU-12. (b) Experimental (solid line) and simulated (dashed line) synchrotron XRD profiles obtained for as-synthesized and calcined KIT-5 mesoporous silica samples, reprinted with permission from ref. 63 and 64. Copyright 2003, Wiley–VCH and American Chemical Society.

to be illustrated by further detailed electron microscopy observation and electron crystallography analysis.

Cubic mesostructure SBA-11 was synthesized by using Brij 56 as a SDA over a wide range of reactant compositions at room temperature. It shows a mean pore size of 2.5–3.6 nm.[36] SBA-11 was reported as a simple cubic $Pm\bar{3}m$ mesostructure according to the poorly resolved XRD patterns. TEM images resolved that SBA-11 has a 3D caged structure. The $Pm\bar{3}m$ mesostructure is the simplest structure due to the uncertainty of cage arrangements.

5.3 Other mesostructures

EI-Safty *et al.*[102,194] reported several 3D mesostructures including $P6_3/mmc$, $Pm\bar{3}m$, $Pn\bar{3}m$, $Pm\bar{3}n$, *etc.* by using microemulsion lyotropic liquid-crystal mesophases of Brij 56 and Brij 76 as templates and alkanes as organic additives under acidic conditions. The XRD patterns, however, are not well resolved, and more intensive characterization is required to resolve these mesostructures.

5.4 Disordered mesostructures

The syntheses of disordered sponge-like or wormhole-like mesoporous silica materials templated by nonionic surfactants have also contributed a great deal to the exploiting of organization principles in the surfactant-templating approach.

Pinnavaia and co-workers developed disordered MSU mesostructures by using nonionic surfactants as templates under neutral conditions.[10,195] Acidic and basic solutions are sometimes adopted. Although the mesostructure is disordered, it has uniformly sized mesopores and high surface areas. This may be one of the reasons for only one broad diffraction peak in the XRD patterns. The pore sizes can be tuned in the range of 2.0–5.8 nm by varying the surfactants. In particular, the pore sizes are very dependent on the synthesis temperature because hydrogen bonds between inorganic species and surfactants under neutral conditions are sensitive to temperature.[113,196,197]

Disordered mesostructures have no unit cell, symmetry and space group. However, the characteristics such as uniform pores, high surface areas, and easy modulation offer them good opportunities in catalysis, adsorption, separation and immobilization.[198–200] Which structure is more benefit in applications, ordered or disordered? It is still hard to pass a definitive verdict due to the complexity.

6 Potential applications

The developments in applications of mesoporous materials lag much behind the achievements in syntheses. More strictly, there is not yet a breakthrough in industrial applications.[7,201] However, vital commercial applications emerge in prospect owing to substantial studies on mesoporous materials, especially on their intrinsic characteristics.

Besides the conventional applications in catalysis, separation and ion-exchange similar to zeolites, mesoporous materials show great potentialities in optics electronics, as well as biological applications. Here we emphasize these novel applications.

6.1 Optical and electronic applications

The most promising commercial prospect of mesoporous materials is expected as low-dielectric constant (low-k) materials in chip fabrication.[7,24] Traditional chips use condensed silicas as dielectrics with k values between 3.9 and 4.2 which can not meet the demands of nanodevices. Low-k materials are thus of urgency.[202] A possible solution is of mesoporous silicates showing k values lower than 2.2.[203] Zhao *et al.*[74] first reported low-k mesoporous silica thin films templated by triblock copolymers with values ranging from 1.45 to 2.1. Larger porosities generally give lower k values for the same mesostructure.[204] As-made or long-time resting mesoporous thin films have high k values by reason of the

polarization of surface silanol groups and the adsorption of water molecules. Hydrophobic treatment of the surface is adopted to obtain low-*k* mesoporous materials.[203]

Marlow *et al.*[205] investigated the optical characteristics of mesoporous silica fibers coated with dye molecules. Due to the amplification of a guided mode in the fibers, directional and gain-narrowed emission can be produced by laser excitation which can be applied as advanced laser materials. On the combination of sol–gel block copolymer templating chemistry with soft lithography, Yang *et al.*[19] fabricated mesoporous silica patterns with low-refractive index. Potential application lies in the fabrication of integrated optical circuits.

The unique function of ordered mesoporous nonsiliceous oxides can also be applied into optical devices. 3D caged mesoporous WO_3–TiO_2 composites exhibit extraordinary electrochromic properties and stable contrast ratios in the wavelength range from 400 to 800 nm. Advanced applications can be achieved in ''smart windows''.[206]

6.2 Bio-applications

Numerous applications of nanomaterials emerge in biology owing to nanosizes matching well with the dimensions of proteins. Low-dimensional nanomaterials (nanoparticles, nanospheres, nanotubes, nanowires and nanobelts) find applications in biomedicines and biotechnologies.[207,208] Novel 3D mesoporous materials are more attractive owing to the synergistic roles of both reaction with biological molecules at surfaces and confinement in regularly arranged nanopores.[201]

Mesostructured inorganic solids manifest outstanding prospects in the fields of protein separation, immobilization, digestion and identification. Since mesoporous molecular sieves were reported to have a sieving role on proteins by Han *et al.*,[209] separation of proteins has been the next goal. Zhao *et al.*[210] utilized mesoporous molecular sieve SBA-15 modified with octadecyltrichlorosilane as a liquid chromatographic substrate. The packing columns exhibit good separation of biological molecules, peptide units and standard protein mixtures (normally the molecular weight of the protein is smaller than 70 000) which are comparable to commercial columns. The separation mechanisms include reversed phase chromatography and the sieving role of SBA-15 due to ordered pore structures and uniform pore sizes.

The stability and reusability of entrapped enzymes inside mesoporous silicates are enhanced for enzymatic hydrolysis of small organic molecules.[211,212] Compared with the conventional supports, mesoporous silicates have advantages of open pore structures, uniform pore distributions and large pore volumes for fixing enzymes.[213] The activities of entrapped enzymes depend mainly on two factors, pore sizes and pore surface.[214,215] Pore sizes should be large enough to entrap the enzymes and the pore surface should have specific affinity to reactants. For example, the modification with mercapto groups on SBA-15 improves the fixation efficiency of trypsins. Desorption of trypsin was found to be low from the confined nanospace.[215]

Protein digestion inside the nanoreactor channels of SBA-15 and FDU-12 was reported by Fan *et al.*[211,212] They found that both proteases and substrates were efficiently captured within these biocompatible nanoreactors. Twelve peptides covering 84% of the protein sequence was revealed after 15 min with an intense signal (signal/noise ratio >80), compared to in-solution tryptic digestion (12 h, 27% protein sequence coverage) (Fig. 22(a)). Fig. 22(b) shows a schematic illustration of proteolysis occuring in nano-confinement of mesoporous silica FDU-12. This class of nanoreactors has been found to simultaneously achieve highly efficient substrate entrapping and unfolding, enzyme flashing, and protein digestion.

Assembling cytochrome *c* guest molecules onto an ordered mesoporous Nb_2O_5 host with a pore size of 6 nm effectively promotes the direct electron transfer of redox proteins.[216] The rapid catalytic response to hydrogen peroxide indicates that the high activity of immobilized biomolecules is retained. Horseradish peroxidase can also be immobilized on a mesoporous Nb_2O_5 host whose high porosity matrix offers a good environment for enzyme loading and substrate diffusion causing high sensitivity and long-term stability. Biosensors based on this type of electrodes exhibit a fast response to the glucose, which have potential applications in biocatalysis for glucose oxidation.

Glass ceramics constituted by CaO–P_2O_5–SiO_2–MO (M = Na, Mg, *etc.*) have been widely studied and used in clinical applications owing to chemical bonding with living bone.[217] Does the mesostructure have any predominance in bone formation? Mesoporous bioactive glasses (MBGs, CaO–P_2O_5–SiO_2) have been synthesized by a simple EISA process in non-aqueous systems.[218] The structures and components of these materials can be easily tuned. The bone-forming activities of MBGs *in vitro* were tested in simulated body fluid to monitor the formation of hydroxycarbonate apatite (HCA) on the surfaces of MBGs as a function of time. Rod-like morphology is shaped after soaking the MBG 80S15C (80S and 15C represent the molar fraction of Si, 80% and Ca, 15%, respectively) for 8 h. However, such a biomimetic morphology has not been molded even after 3 days for the sol–gel-derived BG sample. The better bone-forming bioactivity *in vitro* can be attributed to the higher surface area, larger pore volume and more accessible mesopore surface of the mesostructure than the conventional BG material.

7 Summary and outlook

The development of mesoporous molecular sieves *via* nonionic-surfactant-templating strategy is in its infancy. The goal of creating new family members of mesoporous solids that can find applications in adsorption, catalysis, quantum dots, optics, electrodes and bio-materials will require concerted efforts to develop methods of fabrication, appropriate functionalization, and principles of design.

Nonionic surfactants are effective templates in design and synthesis of mesoporous solids, because of not only low cost and absence of toxicity, but also hydrogen-bonding interactions with precursors and rich mesophase behaviors. For example, large-pore sized mesoporous solids are always templated by block copolymers with high molecular weights.

Synthesis factors are essential for high-quality mesoporous products, including surfactant selection, additives

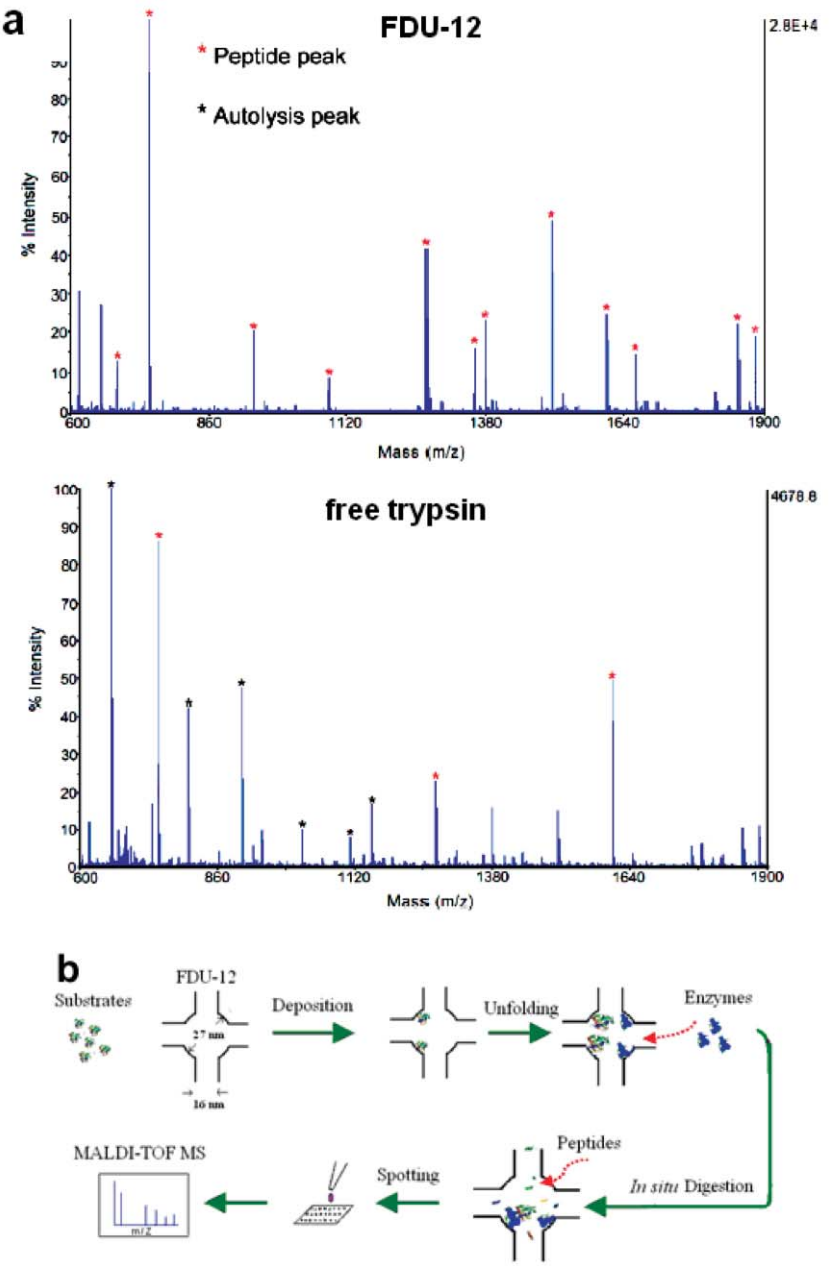

Fig. 22 (a) Matrix-assisted laser desorption/ionization time-of-flight mass spectra obtained from FDU-12 nanopores and solution digestion of myoglobin. Identified peptide peaks (S/N > 80) and tryptic autolysis peaks are labeled with asterisks in red and black, respectively. (b) Schematic illustration for in-nanopore substrate entrapment, unfolding, *in situ* proteolytic digestion, and subsequent MS identification. Reprinted with permission from ref. 212. Copyright 2006, American Chemical Society

(co-surfactants, inorganic additives and organic agents), hydrothermal method (pH value, synthesis temperature and hydrothermal treatment), and EISA strategy. Two main synthesis pathways are demonstrated to design mesoporous solids according to the surfactant-templating approaches. One pathway uses LCT to control the synthesis. In this strategy, the EISA method is shown here as a general method to fabricate highly ordered mesostructured materials. It is highlighted as it skilfully avoids the strong organic–inorganic interaction and facilitates the surfactant-templating approach. A generalized ''acid–base pair'' concept and an organic–organic self-assembly strategy are therefore established. In the former case, the organization of inorganic–organic mesophases is dissociated with the densification of inorganic frameworks while in the preparation of ordered polymers and carbons from organic–organic self-assembly, the cross-linking and thermopolymerization processes of the resols are separated from the assembly. The other pathway is known as a surfactant-templating assembly with inorganic oligomers or nanoparticles, generally using a cooperative formation mechanism. The surfactant-templating assembly and polymerization of inorganic oligomers occur cooperatively and simultaneously.

The nonionic-surfactant-templating approach has the potential to provide the basis for new pathways: (1) utilizing

interfacial tension, (2) controlling common weak interactions other than hydrogen bonds between templates and precursors, such as hydrophobic interaction, and (3) assembling nanoparticles larger than 1 nm. Considerable challenges remain to match the template and inorganic or organic precursors, to create novel mesostructures.

Designed synthesis on the microscale (atoms and molecules) encompasses many classes of materials, such as silicates, organosilicas, metals, sulfides, metal oxides, metal phosphates, metal borates, polymers, carbons, and even inorganic–organic hybrid polymer–silica and carbon–silica nanocomposites. Hydrogen-bonding interaction may facilitate the assembly of nonionic surfactants with diverse precursors. The compositions are more diversified than those derived from either cationic or anionic-surfactant-templating approach.

Typical mesostructures are presented by dividing them into ordered 2D, ordered 3D, disordered and other mesostructures. Potential applications of mesoporous solids particularly in optical devices, electrodes and biomaterials manifest their bright future.

Mesoporous materials from nonionic surfactant-templating approaches face challenges in terms of mesostructures and pore-size limitation. For examples, until now 3D cubic silicate solids with space groups of $Pm\bar{3}n$, $Pn\bar{3}m$, $Fd\bar{3}m$, $Pm\bar{3}m$ have not been obtained by using block copolymers as templates, and uniform, ordered pores are smaller than 30 nm.

The emerging routes will open alternative strategies to new components as well as novel and more complex structures. New surfactants are also expected. Block copolymers tipped with ionic amine head groups may induce the formation of mesostructures and crystalline (microporous) frameworks. ABC triblock copolymers have richer mesophase behaviors and more diverse components compared with ABA-type copolymers. By varying interaction factors (χ_{AB}, χ_{AC} and χ_{BC}) and component factors (f_A and f_B), the hydrophobic/hydrophilic properties of ABC block copolymers can be easily adjusted to form mesostructures such as Q^{214} ($I4_132$), Q^{230} ($Ia\bar{3}2$), O^{70} (*Fddd*) and sponge-like L_3 lamellar structures, which have not so far been observed in mesoporous solids. Self-assembly of A–B diblock copolymers with noncovalent bonds may also yield novel mesostructures.

For the mesopore sizes and shapes, further developments will yield increasing levels of highly ordered mesoporous solids with pore sizes larger than 50 nm, as well as bimodal and hierarchical pores, and chiral pore channels on the basis of suitable block copolymers. Moreover, new synthesis strategies should be explored in order to obtain ordered, large surface area, and thermally stable mesoporous materials especially with semiconductor features such as Si (Ge), metal sulfides, metal nitrides, metal carbides and other compositions that can not be synthesized by the current methods and are desirable in photonic and electronic nanodevices. For example, low-temperature solid-state reaction method and chemical vapor deposition (CVD) on interfaces could be used.

The present syntheses are limited to the qualitative description. With advances in synthesis strategy, fabrication technology, and quantitative illustration from the viewpoint of theoretical and configurable computations, generalized synthetic pathways and rational design of structures, compositions and properties become possible. The development of mesoporous solids will lead to their wide applications in catalysis, sensors, microelectrodes and dielectric materials.

Acknowledgements

This work was supported by NSF of China (20233030, 20373013, 20421303, 20407014 and 20521140450), State Key Basic Research Program of PRC (2006CB202502), Shanghai Sci. & Tech. Committee (03QF14037, 04JC14087, 05DZ22313, 055207078 and 06DJ14006), Shanghai Educational Committee (04DB05), Shanghai Nanotech Promotion Center (0652nm024), Shanghai Leading Academic Discipline Project (T0402), Shanghai HuaYi Chemical Group, and Unilever Research Institute of China. Y. W. thanks the China Post-Doc Scientific Fund.

References

1 J. Yang, M. Mayer, J. K. Kriebel, P. Garstecki and G. M. Whitesides, *Angew. Chem., Int. Ed.*, 2004, **43**, 1555.
2 I. W. Hamley, *Nanotechnology*, 2003, **14**, R39.
3 C. T. Kresge, M. E. Leonowicz, W. J. Roth, J. C. Vartuli and J. S. Beck, *Nature*, 1992, **359**, 710.
4 J. S. Beck, J. C. Vartuli, W. J. Roth, M. E. Leonowicz, C. T. Kresge, K. D. Schmitt, C. T. W. Chu, D. H. Olson, E. W. Sheppard, S. B. McCullen, J. B. Higgins and J. L. Schlenker, *J. Am. Chem. Soc.*, 1992, **114**, 10834.
5 D. Y. Zhao, J. L. Feng, Q. S. Huo, N. Melosh, G. H. Fredrickson, B. F. Chmelka and G. D. Stucky, *Science*, 1998, **279**, 548.
6 A. Stein, B. J. Melde and R. C. Schroden, *Adv. Mater.*, 2000, **12**, 1403.
7 M. E. Davis, *Nature*, 2002, **417**, 813.
8 A. Corma, *Chem. Rev.*, 1997, **97**, 2373.
9 P. T. Tanev and T. J. Pinnavaia, *Science*, 1995, **267**, 865.
10 S. A. Bagshaw, E. Prouzet and T. J. Pinnavaia, *Science*, 1995, **269**, 1242.
11 G. S. Attard, J. C. Glyde and C. G. Goltner, *Nature*, 1995, **378**, 366.
12 M. Templin, A. Franck, A. DuChesne, H. Leist, Y. M. Zhang, R. Ulrich, V. Schadler and U. Wiesner, *Science*, 1997, **278**, 1795.
13 G. M. Whitesides, J. P. Mathias and C. T. Seto, *Science*, 1991, **254**, 1312.
14 Q. S. Huo, D. I. Margolese, U. Ciesla, P. Y. Feng, T. E. Gier, P. Sieger, R. Leon, P. M. Petroff, F. Schuth and G. D. Stucky, *Nature*, 1994, **368**, 317.
15 G. S. Attard, C. G. Goltner, J. M. Corker, S. Henke and R. H. Templer, *Angew. Chem., Int. Ed. Engl.*, 1997, **36**, 1315.
16 S. I. Stupp and P. V. Braun, *Science*, 1997, **277**, 1242.
17 Y. F. Lu, R. Ganguli, C. A. Drewien, M. T. Anderson, C. J. Brinker, W. L. Gong, Y. X. Guo, H. Soyez, B. Dunn, M. H. Huang and J. I. Zink, *Nature*, 1997, **389**, 364.
18 P. D. Yang, D. Y. Zhao, D. I. Margolese, B. F. Chmelka and G. D. Stucky, *Nature*, 1998, **396**, 152.
19 P. D. Yang, G. Wirnsberger, H. C. Huang, S. R. Cordero, M. D. McGehee, B. Scott, T. Deng, G. M. Whitesides, B. F. Chmelka, S. K. Buratto and G. D. Stucky, *Science*, 2000, **287**, 465.
20 Y. Sakamoto, M. Kaneda, O. Terasaki, D. Y. Zhao, J. M. Kim, G. Stucky, H. J. Shim and R. Ryoo, *Nature*, 2000, **408**, 449.
21 D. L. Li, H. S. Zhou and I. Honma, *Nat. Mater.*, 2004, **3**, 65.
22 B. Z. Tian, X. Y. Liu, B. Tu, C. Z. Yu, J. Fan, L. M. Wang, S. H. Xie, G. D. Stucky and D. Y. Zhao, *Nat. Mater.*, 2003, **2**, 159.
23 J. Y. Ying, C. P. Mehnert and M. S. Wong, *Angew. Chem., Int. Ed.*, 1999, **38**, 56.
24 F. Schuth and W. Schmidt, *Adv. Mater.*, 2002, **14**, 629.
25 C. Goltner-Spickermann, *Curr. Opin. Colloid Interface Sci.*, 2002, **7**, 173.
26 A. Stein, *Adv. Mater.*, 2003, **15**, 763.

27 D. Y. Zhao, B. Z. Tian and X. Y. Liu, *Stud. Surf. Sci. Catal.*, 2004, **148**, 139.
28 B. Smarsly and M. Antonietti, *Eur. J. Inorg. Chem.*, 2006, 1111.
29 F. Schuth, *Chem. Mater.*, 2001, **13**, 3184.
30 Y. Wan, H. Yang and D. Zhao, *Acc. Chem. Res.*, 2006, **39**, 423.
31 D. Grosso, G. Soler-Illia, F. Babonneau, C. Sanchez, P. A. Albouy, A. Brunet-Bruneau and A. R. Balkenende, *Adv. Mater.*, 2001, **13**, 1085.
32 P. Alexandridis, U. Olsson and B. Lindman, *Langmuir*, 1998, **14**, 2627.
33 Q. Q. Wang, L. Li and S. P. Jiang, *Langmuir*, 2005, **21**, 9068.
34 S. Forster and M. Antonietti, *Adv. Mater.*, 1998, **10**, 195.
35 C. Z. Yu, J. Fan, B. Z. Tian, G. D. Stucky and D. Y. Zhao, *J. Phys. Chem. B*, 2003, **107**, 13368.
36 D. Y. Zhao, Q. S. Huo, J. L. Feng, B. F. Chmelka and G. D. Stucky, *J. Am. Chem. Soc.*, 1998, **120**, 6024.
37 K. Cassiers, P. Van der Voort, T. Linssen, E. F. Vansant, O. Lebedev and J. Van Landuyt, *J. Phys. Chem. B*, 2003, **107**, 3690.
38 Z. D. Zhang, X. X. Yan, B. Z. Tian, C. Z. Yu, B. Tu, G. S. Zhu, S. L. Qiu and D. Y. Zhao, *Microporous Mesoporous Mater.*, 2006, **90**, 23.
39 P. F. W. Simon, R. Ulrich, H. W. Spiess and U. Wiesner, *Chem. Mater.*, 2001, **13**, 3464.
40 A. C. Finnefrock, R. Ulrich, A. Du Chesne, C. C. Honeker, K. Schumacher, K. K. Unger, S. M. Gruner and U. Wiesner, *Angew. Chem., Int. Ed.*, 2001, **40**, 1207.
41 A. C. Finnefrock, R. Ulrich, G. E. S. Toombes, S. M. Gruner and U. Wiesner, *J. Am. Chem. Soc.*, 2003, **125**, 13084.
42 K. Yu, A. J. Hurd, A. Eisenberg and C. J. Brinker, *Langmuir*, 2001, **17**, 7961.
43 K. Yu, B. Smarsly and C. J. Brinker, *Adv. Funct. Mater.*, 2003, **13**, 47.
44 M. Groenewolt, T. Brezesinski, H. Schlaad, M. Antonietti, P. W. Groh and B. Ivan, *Adv. Mater.*, 2005, **17**, 1158.
45 Y. F. Lu, Y. Yang, A. Sellinger, M. C. Lu, J. M. Huang, H. Y. Fan, R. Haddad, G. Lopez, A. R. Burns, D. Y. Sasaki, J. Shelnutt and C. J. Brinker, *Nature*, 2001, **410**, 913.
46 A. P. Z. Clark, K. F. Shen, Y. F. Rubin and S. H. Tolbert, *Nano Lett.*, 2005, **5**, 1647.
47 F. Y. Tsai, H. L. Tu and C. Y. Mou, *J. Mater. Chem.*, 2006, **16**, 348.
48 B. McCaughey, C. Costello, D. H. Wang, J. E. Hampsey, Z. Z. Yang, C. J. Li, C. J. Brinker and Y. F. Lu, *Adv. Mater.*, 2003, **15**, 1266.
49 P. Kipkemboi, A. Fogden, V. Alfredsson and K. Flodstrom, *Langmuir*, 2001, **17**, 5398.
50 J. L. Blin, A. Leonard and B. L. Su, *Chem. Mater.*, 2001, **13**, 3542.
51 L. M. Wang, H. Fan, B. Z. Tian, H. F. Yang, C. Z. Yu, B. Tu and D. Y. Zhao, *Microporous Mesoporous Mater.*, 2004, **67**, 135.
52 S. S. Kim, A. Karkamkar, T. J. Pinnavaia, M. Kruk and M. Jaroniec, *J. Phys. Chem. B*, 2001, **105**, 7663.
53 Y. Han and J. Y. Ying, *Angew. Chem., Int. Ed.*, 2005, **44**, 288.
54 Y. Han, D. F. Li, L. Zhao, J. W. Song, X. Y. Yang, N. Li, Y. Di, C. J. Li, S. Wu, X. Z. Xu, X. J. Meng, K. F. Lin and F. S. Xiao, *Angew. Chem., Int. Ed.*, 2003, **42**, 3633.
55 X. Y. Liu, B. Z. Tian, C. Z. Yu, F. Gao, S. H. Xie, B. Tu, R. C. Che, L. M. Peng and D. Y. Zhao, *Angew. Chem., Int. Ed.*, 2002, **41**, 3876.
56 K. Flodstrom, V. Alfredsson and N. Kallrot, *J. Am. Chem. Soc.*, 2003, **125**, 4402.
57 F. Kleitz, S. H. Choi and R. Ryoo, *Chem. Commun.*, 2003, 2136.
58 T. W. Kim, F. Kleitz, B. Paul and R. Ryoo, *J. Am. Chem. Soc.*, 2005, **127**, 7601.
59 Y. Q. Wang, C. M. Yang, B. Zibrowius, B. Spliethoff, M. Linden and F. Schuth, *Chem. Mater.*, 2003, **15**, 5029.
60 S. N. Che, A. E. Garcia-Bennett, X. Y. Liu, R. P. Hodgkins, P. A. Wright, D. Y. Zhao, O. Terasaki and T. Tatsumi, *Angew. Chem., Int. Ed.*, 2003, **42**, 3930.
61 B. Z. Tian, X. Y. Liu, L. A. Solovyov, Z. Liu, H. F. Yang, Z. D. Zhang, S. H. Xie, F. Q. Zhang, B. Tu, C. Z. Yu, O. Terasaki and D. Y. Zhao, *J. Am. Chem. Soc.*, 2004, **126**, 865.
62 D. H. Chen, Z. Li, C. Z. Yu, Y. F. Shi, Z. D. Zhang, B. Tu and D. Y. Zhao, *Chem. Mater.*, 2005, **17**, 3228.
63 J. Fan, C. Z. Yu, T. Gao, J. Lei, B. Z. Tian, L. M. Wang, Q. Luo, B. Tu, W. Z. Zhou and D. Y. Zhao, *Angew. Chem., Int. Ed.*, 2003, **42**, 3146.
64 F. Kleitz, D. N. Liu, G. M. Anilkumar, I. S. Park, L. A. Solovyov, A. N. Shmakov and R. Ryoo, *J. Phys. Chem. B*, 2003, **107**, 14296.
65 D. H. Chen, Z. Li, Y. Wan, X. J. Tu, Y. F. Shi, Z. X. Chen, W. Shen, C. Z. Yu, B. Tu and D. Y. Zhao, *J. Mater. Chem.*, 2006, **16**, 1511.
66 P. Y. Feng, X. H. Bu, G. D. Stucky and D. J. Pine, *J. Am. Chem. Soc.*, 2000, **122**, 994.
67 C. Z. Yu, B. Z. Tian, J. Fan, G. D. Stucky and D. Y. Zhao, *J. Am. Chem. Soc.*, 2002, **124**, 4556.
68 J. R. Matos, M. Kruk, L. P. Mercuri, M. Jaroniec, L. Zhao, T. Kamiyama, O. Terasaki, T. J. Pinnavaia and Y. Liu, *J. Am. Chem. Soc.*, 2003, **125**, 821.
69 C. Z. Yu, Y. H. Yu and D. Y. Zhao, *Chem. Commun.*, 2000, 575.
70 D. Coutinho, R. A. Orozio-Tevan, R. F. Reidy and K. J. Balkus, *Microporous Mesoporous Mater.*, 2002, **54**, 229.
71 R. C. Hayward, B. F. Chmelka and E. J. Kramer, *Macromolecules*, 2005, **38**, 7768.
72 Y. T. Chan, H. P. Lin, C. Y. Mou and S. T. Liu, *Chem. Commun.*, 2002, 2878.
73 V. Z. H. Chan, J. Hoffman, V. Y. Lee, H. Iatrou, A. Avgeropoulos, N. Hadjichristidis, R. D. Miller and E. L. Thomas, *Science*, 1999, **286**, 1716.
74 D. Zhao, P. Yang, N. Melosh, J. Feng, B. F. Chmelka and G. D. Stucky, *Adv. Mater.*, 1998, **10**, 1380.
75 B. Z. Tian, X. Y. Liu, Z. D. Zhang, B. Tu and D. Y. Zhao, *J. Solid State Chem.*, 2002, **167**, 324.
76 J. M. Kim, Y. Sakamoto, Y. K. Hwang, Y. U. Kwon, O. Terasaki, S. E. Park and G. D. Stucky, *J. Phys. Chem. B*, 2002, **106**, 2552.
77 F. Kleitz, J. Blanchard, B. Zibrowius, F. Schuth, P. Agren and M. Linden, *Langmuir*, 2002, **18**, 4963.
78 T. Brezesinski, C. Erpen, K. Iimura and B. Smarsly, *Chem. Mater.*, 2005, **17**, 1683.
79 O. Sel, D. B. Kuang, M. Thommes and B. Smarsly, *Langmuir*, 2006, **22**, 2311.
80 M. Groenewolt, M. Antonietti and S. Polarz, *Langmuir*, 2004, **20**, 7811.
81 K. Suzuki, K. Ikari and H. Imai, *J. Am. Chem. Soc.*, 2004, **126**, 462.
82 R. Ryoo, S. H. Joo and J. M. Kim, *J. Phys. Chem. B*, 1999, **103**, 7435.
83 C. Z. Yu, J. Fan, B. Z. Tian and D. Y. Zhao, *Chem. Mater.*, 2004, **16**, 889.
84 C. Z. Yu, B. Z. Tian, B. Fan, G. D. Stucky and D. Y. Zhao, *Chem. Commun.*, 2001, 2726.
85 E. Leontidis, *Curr. Opin. Colloid Interface Sci.*, 2002, **7**, 81.
86 H. P. Lin and C. Y. Mou, *Acc. Chem. Res.*, 2002, **35**, 927.
87 S. N. Che, H. C. Li, S. Lim, Y. Sakamoto, O. Terasaki and T. Tatsumi, *Chem. Mater.*, 2005, **17**, 4103.
88 J. W. Tang, C. Z. Yu, X. F. Zhou, X. X. Yan and D. Y. Zhao, *Chem. Commun.*, 2004, 2240.
89 D. Y. Zhao, P. D. Yang, B. F. Chmelka and G. D. Stucky, *Chem. Mater.*, 1999, **11**, 1174.
90 C. Z. Yu, J. Fan and D. Y. Zhao, *Acta Chim. Sinica*, 2002, **60**, 1357.
91 K. Landskron, B. D. Hatton, D. D. Perovic and G. A. Ozin, *Science*, 2003, **302**, 266.
92 W. P. Guo, J. Y. Park, M. O. Oh, H. W. Jeong, W. J. Cho, I. Kim and C. S. Ha, *Chem. Mater.*, 2003, **15**, 2295.
93 J. P. Hanrahan, M. P. Copley, K. M. Ryan, T. R. Spalding, M. A. Morris and J. D. Holmes, *Chem. Mater.*, 2004, **16**, 424.
94 Z. Konya, V. F. Puntes, I. Kiricsi, J. Zhu, A. P. Alivisatos and G. A. Somorjai, *Nano Lett.*, 2002, **2**, 907.
95 Q. Y. Hu, J. E. Hampsey, N. Jiang, C. J. Li and Y. F. Lu, *Chem. Mater.*, 2005, **17**, 1561.
96 J. L. Ruggles, E. P. Gilbert, S. A. Holt, P. A. Reynolds and J. W. White, *Langmuir*, 2003, **19**, 793.
97 J. S. Lettow, Y. J. Han, P. Schmidt-Winkel, P. D. Yang, D. Y. Zhao, G. D. Stucky and J. Y. Ying, *Langmuir*, 2000, **16**, 8291.
98 J. L. Blin and B. L. Su, *Langmuir*, 2002, **18**, 5303.
99 S. K. Jana, R. Nishida, K. Shindo, T. Kugita and S. Namba, *Microporous Mesoporous Mater.*, 2004, **68**, 133.

100 J. Fan, C. Z. Yu, J. Lei, Q. Zhang, T. C. Li, B. Tu, W. Z. Zhou and D. Y. Zhao, *J. Am. Chem. Soc.*, 2005, **127**, 10794.
101 S. A. El-Safty, T. Hanaoka and F. Mizukami, *Chem. Mater.*, 2005, **17**, 3137.
102 S. A. El-Safty and T. Hanaoka, *Chem. Mater.*, 2004, **16**, 384.
103 Q. Y. Sun, P. J. Kooyman, J. G. Grossmann, P. H. H. Bomans, P. M. Frederik, P. Magusin, T. P. M. Beelen, R. A. van Santen and N. Sommerdijk, *Adv. Mater.*, 2003, **15**, 1097.
104 H. F. Yang, Q. H. Shi, B. Z. Tian, S. H. Xie, F. Q. Zhang, Y. Yan, B. Tu and D. Y. Zhao, *Chem. Mater.*, 2003, **15**, 536.
105 D. Y. Zhao, J. Y. Sun, Q. Z. Li and G. D. Stucky, *Chem. Mater.*, 2000, **12**, 275.
106 N. R. B. Coleman and G. S. Attard, *Microporous Mesoporous Mater.*, 2001, **44**, 73.
107 M. A. U. Martines, E. Yeong, A. Larbot and E. Prouzet, *Microporous Mesoporous Mater.*, 2004, **74**, 213.
108 M. J. Yuan, J. W. Tang, C. Z. Yu, Y. H. Chen, B. Tu and D. Y. Zhao, *Chem. Lett.*, 2003, **32**, 660.
109 A. C. Voegtlin, F. Ruch, J. L. Guth, J. Patarin and L. Huve, *Microporous Mater.*, 1997, **9**, 95.
110 J. M. Kim, Y. J. Han, B. F. Chmelka and G. D. Stucky, *Chem. Commun.*, 2000, 2437.
111 F. Kleitz, L. A. Solvyov, G. M. Anilkumar, S. H. Choi and R. Ryoo, *Chem. Commun.*, 2004, 1536.
112 F. Kleitz, T. W. Kim and R. Ryoo, *Langmuir*, 2006, **22**, 440.
113 C. Boissiere, A. Larbot, C. Bourgaux, E. Prouzet and C. A. Bunton, *Chem. Mater.*, 2001, **13**, 3580.
114 D. Y. Zhao, C. Nie, Y. M. Zhou, S. J. Xia, L. M. Huang and Q. Z. Li, *Catal. Today*, 2001, **68**, 11.
115 B. L. Newalkar, S. Komarneni, U. T. Turaga and H. Katsuki, *J. Mater. Chem.*, 2003, **13**, 1710.
116 P. F. Fulvio, S. Pikus and M. Jaroniec, *J. Mater. Chem.*, 2005, **15**, 5049.
117 A. Galarneau, N. Cambon, F. Di Renzo, R. Ryoo, M. Choi and F. Fajula, *New J. Chem.*, 2003, **27**, 73.
118 C. Z. Yu, B. H. Tian, J. Fan, G. D. Stucky and D. Y. Zhao, *Chem. Lett.*, 2002, 62.
119 G. J. D. Soler-illia, C. Sanchez, B. Lebeau and J. Patarin, *Chem. Rev.*, 2002, **102**, 4093.
120 D. Grosso, F. Cagnol, G. Soler-Illia, E. L. Crepaldi, H. Amenitsch, A. Brunet-Bruneau, A. Bourgeois and C. Sanchez, *Adv. Funct. Mater.*, 2004, **14**, 309.
121 E. L. Crepaldi, G. Soler-Illia, D. Grosso, F. Cagnol, F. Ribot and C. Sanchez, *J. Am. Chem. Soc.*, 2003, **125**, 9770.
122 B. Smarsly, G. Xomeritakis, K. Yu, N. G. Liu, H. Y. Fan, R. A. Assink, C. A. Drewien, W. Ruland and C. J. Brinker, *Langmuir*, 2003, **19**, 7295.
123 Q. S. Huo, D. I. Margolese and G. D. Stucky, *Chem. Mater.*, 1996, **8**, 1147.
124 D. Grosso, A. R. Balkenende, P. A. Albouy, A. Ayral, H. Amenitsch and F. Babonneau, *Chem. Mater.*, 2001, **13**, 1848.
125 B. Smarsly, A. Gibaud, W. Ruland, D. Sturmayr and C. J. Brinker, *Langmuir*, 2005, **21**, 3858.
126 B. Z. Tian, H. F. Yang, X. Y. Liu, S. H. Xie, C. Z. Yu, J. Fan, B. Tu and D. Y. Zhao, *Chem. Commun.*, 2002, 1824.
127 P. Y. Feng, X. H. Bu, T. E. Gier and G. D. Stucky, *Microporous Mesoporous Mater.*, 1998, **23**, 221.
128 R. A. Pai, R. Humayun, M. T. Schulberg, A. Sengupta, J. N. Sun and J. J. Watkins, *Science*, 2004, **303**, 507.
129 S. A. Davis, M. Breulmann, K. H. Rhodes, B. Zhang and S. Mann, *Chem. Mater.*, 2001, **13**, 3218.
130 D. M. Antonelli and J. Y. Ying, *Angew. Chem., Int. Ed. Engl.*, 1995, **34**, 2014.
131 S. Ruthstein, V. Frydman, S. Kababya, M. Landau and D. Goldfarb, *J. Phys. Chem. B*, 2003, **107**, 1739.
132 S. Ruthstein, J. Schmidt, E. Kesselman, Y. Talmon and D. Goldfarb, *J. Am. Chem. Soc.*, 2006, **128**, 3366.
133 K. Flodstrom, H. Wennerstrom and V. Alfredsson, *Langmuir*, 2004, **20**, 680.
134 A. Y. Khodakov, V. L. Zholobenko, M. Imperor-Clerc and D. Durand, *J. Phys. Chem. B*, 2005, **109**, 22780.
135 Z. H. Luan, C. F. Cheng, W. Z. Zhou and J. Klinowski, *J. Phys. Chem.*, 1995, **99**, 1018.
136 Y. Wan, J. X. Ma, Z. Wang, W. Zhou and S. Kaliaguine, *J. Catal.*, 2004, **227**, 242.
137 A. Vinu, D. P. Sawant, K. Ariga, K. Z. Hossain, S. B. Halligudi, M. Hartmann and M. Nomura, *Chem. Mater.*, 2005, **17**, 5339.
138 A. Vinu, P. Srinivasu, M. Miyahara and K. Ariga, *J. Phys. Chem. B*, 2006, **110**, 801.
139 Z. El Berrichi, L. Cherif, O. Orsen, J. Fraissard, J. P. Tessonnier, E. Vanhaecke, B. Louis, M. J. Ledoux and C. Pham-Huu, *Appl. Catal., A*, 2006, **298**, 194.
140 J. Trebosc, J. W. Wiench, S. Huh, V. S. Y. Lin and M. Pruski, *J. Am. Chem. Soc.*, 2005, **127**, 7587.
141 R. J. P. Corriu, A. Mehdi and C. Reye, *J. Mater. Chem.*, 2005, **15**, 4285.
142 D. Margolese, J. A. Melero, S. C. Christiansen, B. F. Chmelka and G. D. Stucky, *Chem. Mater.*, 2000, **12**, 2448.
143 M. Kruk, T. Asefa, N. Coombs, M. Jaroniec and G. A. Ozin, *J. Mater. Chem.*, 2002, **12**, 3452.
144 C. M. Yang, Y. Q. Wang, B. Zibrowius and F. Schuth, *Phys. Chem. Chem. Phys.*, 2004, **6**, 2461.
145 B. Hatton, K. Landskron, W. Whitnall, D. Perovic and G. A. Ozin, *Acc. Chem. Res.*, 2005, **38**, 305.
146 F. Hoffmann, M. Cornelius, J. Morell and M. Froba, *J. Nanosci. Nanotechnol.*, 2006, **6**, 265.
147 O. Muth, C. Schellbach and M. Froba, *Chem. Commun.*, 2001, 2032.
148 S. Hamoudi and S. Kaliaguine, *Chem. Commun.*, 2002, 2118.
149 M. P. Kapoor and S. Inagaki, *Chem. Mater.*, 2002, **14**, 3509.
150 A. Sayari and W. H. Wang, *J. Am. Chem. Soc.*, 2005, **127**, 12194.
151 W. J. Hunks and G. A. Ozin, *Chem. Mater.*, 2004, **16**, 5465.
152 O. Olkhovyk and M. Jaroniec, *J. Am. Chem. Soc.*, 2005, **127**, 60.
153 K. Landskron and G. A. Ozin, *Science*, 2004, **306**, 1529.
154 P. V. Braun, P. Osenar and S. I. Stupp, *Nature*, 1996, **380**, 325.
155 B. M. Rabatic, M. U. Pralle, G. N. Tew and S. I. Stupp, *Chem. Mater.*, 2003, **15**, 1249.
156 P. A. Nelson, J. M. Elliott, G. S. Attard and J. R. Owen, *Chem. Mater.*, 2002, **14**, 524.
157 I. Nandhakumar, J. M. Elliott and G. S. Attard, *Chem. Mater.*, 2001, **13**, 3840.
158 G. S. Attard, S. A. A. Leclerc, S. Maniguet, A. E. Russell, I. Nandhakumar and P. N. Bartlett, *Chem. Mater.*, 2001, **13**, 1444.
159 W. H. J. Hogarth, J. C. D. da Costa, J. Drennan and G. Q. Lu, *J. Mater. Chem.*, 2005, **15**, 754.
160 M. Eswaramoorthy, S. Neeraj and C. N. R. Rao, *Microporous Mesoporous Mater.*, 1999, **28**, 205.
161 S. D. Shen, B. Z. Tian, C. Z. Yu, S. H. Xie, Z. D. Zhang, B. Tu and D. Y. Zhao, *Chem. Mater.*, 2003, **15**, 4046.
162 U. Ciesla, M. Froba, G. Stucky and F. Schuth, *Chem. Mater.*, 1999, **11**, 227.
163 Y. Z. Khimyak and J. Klinowski, *J. Chem. Soc., Faraday Trans.*, 1998, **94**, 2241.
164 M. Tiemann and M. Froba, *Chem. Mater.*, 2001, **13**, 3211.
165 T. Kimura, *Chem. Mater.*, 2005, **17**, 5521.
166 R. Ryoo, S. H. Joo and S. Jun, *J. Phys. Chem. B*, 1999, **103**, 7743.
167 A. S. Zalusky, R. Olayo-Valles, J. H. Wolf and M. A. Hillmyer, *J. Am. Chem. Soc.*, 2002, **124**, 12761.
168 J. Jang and J. Bae, *Chem. Commun.*, 2005, 1200.
169 C. D. Liang, K. L. Hong, G. A. Guiochon, J. W. Mays and S. Dai, *Angew. Chem., Int. Ed.*, 2004, **43**, 5785.
170 S. Tanaka, N. Nishiyama, Y. Egashira and K. Ueyama, *Chem. Commun.*, 2005, 2125.
171 Y. Meng, D. Gu, F. Q. Zhang, Y. F. Shi, H. F. Yang, Z. Li, C. Z. Yu, B. Tu and D. Y. Zhao, *Angew. Chem., Int. Ed.*, 2005, **44**, 7053.
172 Y. Meng, D. Gu, F. Q. Zhang, Y. F. Shi, L. Cheng, D. Feng, Z. X. Wu, Z. X. Chen, Y. Wan, A. Stein and D. Y. Zhao, *Chem. Mater.*, 2006, **18**, 4447.
173 F. Q. Zhang, Y. Meng, D. Gu, Y. Yan, C. Z. Yu, B. Tu and D. Y. Zhao, *J. Am. Chem. Soc.*, 2005, **127**, 13508.
174 R. L. Liu, Y. F. Shi, Y. Wan, Y. Meng, F. Q. Zhang, D. Gu, Z. X. Chen, B. Tu and D. Y. Zhao, *J. Am. Chem. Soc.*, 2006, **128**, 11652.
175 D. Grosso, G. Soler-Illia, E. L. Crepaldi, F. Cagnol, C. Sinturel, A. Bourgeois, A. Brunet-Bruneau, H. Amenitsch, P. A. Albouy and C. Sanchez, *Chem. Mater.*, 2003, **15**, 4562.
176 T. Katou, B. Lee, D. L. Lu, J. N. Kondo, M. Hara and K. Domen, *Angew. Chem., Int. Ed.*, 2003, **42**, 2382.

177 K. Miyazawa and S. Inagaki, *Chem. Commun.*, 2000, 2121.
178 H. F. Yang and D. Y. Zhao, *J. Mater. Chem.*, 2005, **15**, 1217.
179 R. Ryoo, S. H. Joo, M. Kruk and M. Jaroniec, *Adv. Mater.*, 2001, **13**, 677.
180 J. Fan, C. Z. Yu, L. M. Wang, B. Tu, D. Y. Zhao, Y. Sakamoto and O. Terasaki, *J. Am. Chem. Soc.*, 2001, **123**, 12113.
181 R. Ryoo, C. H. Ko, M. Kruk, V. Antochshuk and M. Jaroniec, *J. Phys. Chem. B*, 2000, **104**, 11465.
182 V. T. Hoang, Q. L. Huang, M. Eic, T. O. Do and S. Kaliaguine, *Langmuir*, 2005, **21**, 2051.
183 H. Vinh-Thang, Q. L. Huang, M. Eic, D. Trong-On and S. Kaliaguine, *Langmuir*, 2005, **21**, 5094.
184 F. Q. Zhang, Y. Yan, H. F. Yang, Y. Meng, C. Z. Yu, B. Tu and D. Y. Zhao, *J. Phys. Chem. B*, 2005, **109**, 8723.
185 B. Z. Tian, X. Y. Liu, H. F. Yang, S. H. Xie, C. Z. Yu, B. Tu and D. Y. Zhao, *Adv. Mater.*, 2003, **15**, 1370.
186 P. I. Ravikovitch and A. V. Neimark, *Langmuir*, 2002, **18**, 1550.
187 P. Van der Voort, M. Benjelloun and E. F. Vansant, *J. Phys. Chem. B*, 2002, **106**, 9027.
188 T. W. Kim, R. Ryoo, M. Kruk, K. P. Gierszal, M. Jaroniec, S. Kamiya and O. Terasaki, *J. Phys. Chem. B*, 2004, **108**, 11480.
189 C. M. Yang, W. Schmidt and F. Kleitz, *J. Mater. Chem.*, 2005, **15**, 5112.
190 M. Kruk, E. B. Celer, J. R. Matos, S. Pikus and M. Jaroniec, *J. Phys. Chem. B*, 2005, **109**, 3838.
191 R. M. Grudzien and M. Jaroniec, *Chem. Commun.*, 2005, 1076.
192 M. Kruk, E. B. Celer and M. Jaroniec, *Chem. Mater.*, 2004, **16**, 698.
193 Y. Sakamoto, I. Diaz, O. Terasaki, D. Y. Zhao, J. Perez-Pariente, J. M. Kim and G. D. Stucky, *J. Phys. Chem. B*, 2002, **106**, 3118.
194 S. A. El-Safty and T. Hanaoka, *Chem. Mater.*, 2003, **15**, 2892.
195 E. Prouzet, F. Cot, G. Nabias, A. Larbot, P. Kooyman and T. J. Pinnavaia, *Chem. Mater.*, 1999, **11**, 1498.
196 G. Herrier, J. L. Blin and B. L. Su, *Langmuir*, 2001, **17**, 4422.
197 J. L. Blin, A. Leonard and B. L. Su, *J. Phys. Chem. B*, 2001, **105**, 6070.
198 J. C. Jansen, Z. Shan, L. Marchese, W. Zhou, N. von der Puil and T. Maschmeyer, *Chem. Commun.*, 2001, 713.
199 R. Mokaya, W. Jones, S. Moreno and G. Poncelet, *Catal. Lett.*, 1997, **49**, 87.
200 P. M. Price, J. H. Clark and D. J. Macquarrie, *J. Chem. Soc., Dalton Trans.*, 2000, 101.
201 M. Antonietti and G. A. Ozin, *Chem. Eur. J.*, 2004, **10**, 29.
202 R. D. Miller, *Science*, 1999, **286**, 421.
203 S. Baskaran, J. Liu, K. Domansky, N. Kohler, X. H. Li, C. Coyle, G. E. Fryxell, S. Thevuthasan and R. E. Williford, *Adv. Mater.*, 2000, **12**, 291.
204 H. Y. Fan, F. Van Swol, Y. F. Lu and C. J. Brinker, *J. Non-Cryst. Solids*, 2001, **285**, 71.
205 F. Marlow, M. D. McGehee, D. Y. Zhao, B. F. Chmelka and G. D. Stucky, *Adv. Mater.*, 1999, **11**, 632.
206 M. J. Yuan, Y. D. Lu, B. Z. Tian, H. F. Yang, B. Tu, J. Kong and D. Y. Zhao, *Chem. Lett.*, 2004, **33**, 1396.
207 C. R. Martin and P. Kohli, *Nat. Rev. Drug Discov.*, 2003, **2**, 29.
208 H. R. Luckarift, J. C. Spain, R. R. Naik and M. O. Stone, *Nat. Biotechnol.*, 2004, **22**, 211.
209 Y. J. Han, G. D. Stucky and A. Butler, *J. Am. Chem. Soc.*, 1999, **121**, 9897.
210 J. W. Zhao, F. Gao, Y. L. Fu, W. Jin, P. Y. Yang and D. Y. Zhao, *Chem. Commun.*, 2002, 752.
211 J. Fan, W. Q. Shui, P. Y. Yang, X. Y. Wang, Y. M. Xu, H. H. Wang, X. Chen and D. Y. Zhao, *Chem. Eur. J.*, 2005, **11**, 5391.
212 W. Q. Shui, J. Fan, P. Y. Yang, C. L. Liu, J. J. Zhai, J. Lei, Y. Yan, D. Y. Zhao and X. Chen, *Anal. Chem.*, 2006, **78**, 4811.
213 H. H. P. Yiu and P. A. Wright, *J. Mater. Chem.*, 2005, **15**, 3690.
214 J. Deere, E. Magner, J. G. Wall and B. K. Hodnett, *Chem. Commun.*, 2001, 465.
215 H. H. P. Yiu, P. A. Wright and N. P. Botting, *J. Mol. Catal. B*, 2001, **15**, 81.
216 X. Xu, B. Z. Tian, J. L. Kong, S. Zhang, B. H. Liu and D. Y. Zhao, *Adv. Mater.*, 2003, **15**, 1932.
217 L. L. Hench and J. M. Polak, *Science*, 2002, **295**, 1014.
218 X. X. Yan, C. Z. Yu, X. F. Zhou, J. W. Tang and D. Y. Zhao, *Angew. Chem., Int. Ed.*, 2004, **43**, 5980.

